A mathematical modeling toolbox for ion channels and transporters across cell membranes

Shadi Zaheri[a], Fatemeh Hassanipour[a,*]

[a]*Department of Mechanical Engineering, The University of Texas at Dallas, Richardson, TX, 75080, USA*

Abstract

Mathematical modeling of membrane transporters and ion channels helps researchers obtain a thorough understanding of the complex regulation process between membrane transporters, estimate the changes and uncertainties of their mechanisms, and study how disorders in these procedures may cause disease. A unified mathematical framework that includes most available models for ion channels and transporters can help scientists choose the appropriate model more conveniently. In this regard, this work presents a comprehensive, up-to-date set of currently available mathematical equations for modeling ion channel and membrane transporter mechanisms. This paper aims to provide a mathematical framework for modeling molecule transport, such as nutrients, inorganic ions, drugs, and toxins, across the cell through membrane transporters and ion channels. Our purpose is to substantially save the time and resources needed to find the mathematical models available for different classes of membrane transporters and improve communication between scientists with different backgrounds interested in this field.

Keywords: Membrane transporter models, Ion channel models, Kinetic modeling of membrane transporter

⋆This document is the result of the research project funded by the National Science Foundation.

*Corresponding author

Email addresses: shadi.zaheri@utdallas.edu (Shadi Zaheri), fatemeh@utdallas.edu (Fatemeh Hassanipour)

.

Nomenclature

Conventions

Square brackets: Typically are used with letters (e.g., [A], [B], [EA]) to indicate the concentration of the substrate.

Subscripts E and its compounds (e.g., ENa, ECl, ENaCl): When used with reaction or transport quantities (e.g., reaction rate constants, translocation rate, concentration, flux), these refer to carrier and to the carrier-substrate complex, respectively.

Superscripts o and i: When used with reaction or transport quantities (e.g., concentration, flux), these refer to the transport domain in a system with multiple domains (i.e., outside the cell or inside the cell, l: luminal, 'i,c': intracellular, bl: basolateral).

Physics Constants

F	Faraday's constant	$96,490 \quad (A \cdot s/mol)$
R	Universal gas constant	$8.314 \quad (J/(mol \cdot K))$

Abbreviations

AAT Amino Acid Transporters

$CaCC$ **C**alcium dependent **C**hloride **C**hannel

$CaKC$ **C**alcium-**A**ctivated Potassium (**K**) **C**hannels

$CFTR$ **C**ystic **F**ibrosis **T**ransmembrane conductance **R**egulator

$ENaC$ **E**pithelial Sodium (**Na**) **C**hannels

$H-ATPase$ Proton ATPase

$H/KATPase$ Hydrogen-Potassium ATPase

$IRKC$ **I**nward-**R**ectifier Potassium (**K**) **C**hannels

$K2P$ **T**wo-**P**ore-domain potassium (**K**) channel

$KATP$ **ATP**-sensitive Potassium (**K**) Channel

KCC Chloride Potassium Cotransporter

$NaKATPase$ Sodium Potassium ATPase pump

NBC Sodium Bicarbonate Cotransporter

NCC Sodium Chloride Cotransporter

NCX Sodium Calcium Exchanger

NHE Sodium Hydrogen Exchanger

$NKCC$ Sodium Potassium Chloride Cotransporter

$PMCA$ **P**lasma **M**embrane **C**alcium **A**TPase

$SERCA$ **S**acro **E**ndoplasmic **R**eticulum **C**alcium **A**TPase

$SGLT$ Sodium Glucose Symporter

SOC **S**tore **O**perated **C**hannels

$VGPC$ **V**oltage **G**ated **P**otassium **C**hannel

$VGSC$ **V**oltage **G**ated **S**odium **C**hannel ($VGSC$, Na_v, $VONa$)

Greek symbols

η_h Hill coefficient

Other Symbols

$[Ca]_{er}$ The calcium concentration in the endoplasmic reticulum (ER)

$[Ca]_{sr}$ The calcium concentration in the smooth endoplasmic reticulum (SR)

$\bar{f}_o^{Kv}$ The steady state open probability of the K_v channel

η_{CaKC} The Hill coefficient for the CaKC open probability

η_{SERCA} The Hill coefficient for the SERCA pump

$\overline{C_i}$ Volume-averaged molar concentration of species $'i'$

$\overline{P}_{Ca,CaL}^{M-N}$ The permeability coefficient for the calcium ions through the Ca_L channels

$\mathbf{E}$ Electric field

C_i Molar concentration of species $'i'$

C_L The concentration of unbound ligand for the Hill model

D_i Diffusion coefficient of species $'i'$

$f_d^{Ca_l}$ The inactivation probability of calcium L-type channels

$f_o^{Ca_l}$ The activation probability of calcium L-type channels

$f_o^{channel}$ Open probability of the ion channel

$f_o^{K,CaKC}$ The open probability for CaKC channels

$f_o^{k,kir}$ The open probability of these channels

f_o^{KATP} The open probability for KATP channels at a given ATP concentration

f_o^{SOC} The open probability for SOC channels

f_o^{SOC} The open probability of the SOC channels

$F_{convection}$ Axial volumetric convection fluid flow rate in the tube

$f_o^{Cl,CaCC}$ The open probability of the CaCC channels

g When used in the carrier-mediated transport equations (e.g., $g_A^M, g)B^M$), it indicates the translocation rate constant

$g_{Ca,SOC}^{max}$ The maximum cell conductance for calcium ions through SOC channels

$g_{Ca_L}^{max}$ The maximum cell conductance for calcium L-type channels

g_{CaKC} The maximum whole-cell conductance for the CaKC channels

g_{Cl} the maximum whole cell conductance for chloride anions

$g_{i,channel}$ Membrane conductance for channels of ion $'i'$ (channel conductance)

g_{K_v} The cell conductance for K_v channels

g_{KATP} The cell conductance for the KATP channels

g_{kir} The cell conductance for potassium ions through IRKC channels

g_{NaC} The membrane conductance for sodium channels

$I''_{i,channel}$ Net current density of ion $'i'$ through the ion channels

I_{NaK}^{max} The maximum NaK ATPase current

I_{NCX}^{max} The maximal NCX current flux in ($\mu A \mu F$)

I_{SERCA}^{max} The maximum current through the SERCA pump

$J_{antiporter}$ The transported flux driven via antiporters

J_{ATPase} The transported flux driven via ATPase pumps

$J_{H,HATPase}^{max}$ The maximum hydrogen flux through $H - ATPase$ pumps

$J_{ionchannel}$ The ion flux through the ion channels

$J_{Na^+}^{NakATpase}$ The maximum steady-state efflux of the sodium ions

j_{Na_v} The slow inactivation gates of the Na_v

$J_{symporter}$ The transported flux driven via symporters

$J_{uniporter}$ The transported flux driven via uniporters

$J_{waterchannel}$ The water flux through the water channels

K When used in the carrier-mediated transport equations (e.g., $K_A^M = k_A^{-M}/k_A^{+M}$, $K_B^M = k_B^{-M}/k_B^{+N}$), it indicates the dissociation constant for a reaction step.

k^+ Binding rate constant (e.g., k_A^+ is the binding constant for solute A)

k^- Unbinding rate constant (e.g., k_A^- is the unbinding constant for solute A)

K_A The ligand concentration at which half-saturation is achieved, for Hill model

K_i^M Equilibrium constant coefficient for substrate $'i'$ in domain M

K_m Michaelis-Menten rate constant, which is the substrate concentration at half the maximum rate (V_{max})

K_{Ca}^{CaKC} Potassium concentration at half of the maximum reaction rate for the CaKC open probability

K_{ion} The ion dissociation constant of the ion

k_{kir} The inward rectifier constant(the steepness factor of conductance-voltage relationship)

K_K^{NaK} The saturation constants for the extracellular potassium ions

K_{Na}^{NaK} The saturation constants for the intracellular sodium ions

$O_i^{channel}$ The total number of open channels per unit area of the membrane

P_i^m Membrane permeability coefficient to the solute $'i'$

$P^{M-N(a)}_{Ca,SOC}$ The apical membrane permeability coefficient for the calcium through SOC channels

$P^{M-N(a)}_{Cl,CFTR}$ The permeability coefficient for the CFTR channel

P_{Cl/HCO_3} The permeability of the membrane to the Cl/HCO_3 exchanger per unit area of the membrane

$P^{M-N}_{K,K2P}$ The membrane permeability for potassium ions through a single K2P

$P^{M-N}_{K,X_{CaKC}}$ The permeability coefficient for the potassium ions through the CaKC channels

$P^{M-N(a)}_{Na,ENaC}$ The permeability coefficient for the sodium ions through the ENaC channels

$P^{M-N(a)}_{Na,SOC}$ The apical membrane permeability coefficient for the sodium ions through SOC channels

T Temperature

V^{M-N}_{K} The Nernst equilibrium potential for potassium ions

V_m Membrane voltage or membrane electric potential

$V^{Ca_l,M-N}_{1/2,f_d}$ The half-activation potentials for Ca_l channels

$V^{Ca_l,M-N}_{1/2,f_o}$ The half-inactivation potentials for Ca_l channels

$V_{1/2,Kir}$ The half-activation potential

$V^{M-N}_{Ca,rev}$ The Nernst equilibrium potential of calcium ions

V^{M-N}_{Cl} The Nernest potential for the chloride ions

$V_{i,rev}$ Membrane reversal potential for a single ion $'i'$

V_{max} Maximum reaction velocity achieved at the saturated substrate concentrations for the Michaelis-Menten model

V^{M-N}_{Na} The Nernst equilibrium potential of Na ions

z_i Ionic charge number on an ion $'i'$

h_{Ca_t} The inactivation gating component of the Ca_L channels

h_{Na_v} The inactivation component of the Na_v channel

K_{Ki} The NaKATPase pump affinity for potassium ions

K_{Nai} The NaKATPase pump affinity for sodium ions

m_{Ca_t} The activation gating component of the Ca_L channels

m_{Na_v} The activation component of the Na_v channel

n''^{M-N}_{CaCC} The CaCC channel density per membrane area

n''^{M-N}_{CaKC} The number of CaKC channel density per unit area of the membrane

$n''^{M-N(a)}_{CFTR}$ The CFTR channel density per membrane area

n''_{NaC} Density per area of the NaCC channel

1. Introduction

Ion channels and membrane transporters, including symporters, antiporters, and pumps, are essential determinants for biological processes that involve nutrition, signaling, neurotransmission, cell communication, and drug uptake or efflux [1–4]. Dysfunctionalities in membrane transporter operation can contribute to the development of diseases, such as diabetes, cystic fibrosis, cardiovascular disease, chronic disease, and several other complex diseases [5–9]. Therefore, it is essential to have a better understanding of membrane transporter mechanisms and their underlying operating conditions. Both experimental and mathematical/computational methods are required to understand these mechanisms, and both categories are not mutually exclusive. Mathematical models can be combined with quantitative experiments and use the underlying physiology to reproduce the system's known data. They are particularly useful for identifying drug targets because they provide multiple perturbations or multiple knockouts to be tested in silico without the need for carefully controlled inhibitor dosing studies [10]. Kinetic models are one type of membrane transporter mathematical model that can help estimate the conformational transitions between distinct

states. These models explain how solute carriers utilize the electrochemical gradient to establish and maintain a substrate gradient. Kinetic models also provide realistic quantitative predictions of the substrate flux transported by transporters under initial conditions and at steady-state conditions [4, 11]. They allow for predicting the intra- and extracellular substrate concentrations maintained by a transporter at steady state when the conversion efficiency between the driving solute's electrochemical gradient and the substrate is low [11, 12].

Mathematical models of the kinetic mechanisms of transporters are often developed using biochemical models, kinetic equations, Hill expression, and Michaelis-Menten equations [13, 14]. Modeling these mechanisms is challenged by the incredible diversity of binding order, in which kinetic parameters are mostly unknown. Furthermore, these mathematical models are mostly valid with the assumptions that generated them. Therefore, there is a need to identify the fundamental mechanisms constraining the transport flux rates by membrane transporters and the available data for the set of parameters needed to use these models [15].

In regard to ion channels, ion channels' electrophysiological models are widely developed using Ohm's Law, mass-action kinetics, and Goldman-Hodgkin equations. In using the nonlinear Goldman-Hodgkin model, the diffusion coefficient and the electrokinetic mobility of the ion through the ion channels are the controlling parameters. The linear Ohmic model requires the specification of the membrane electric conductance to the studied ion.

Over several decades, many different channels and transporter models have been developed for various cell types, organs, and tissues [5, 12, 16–18]. The models for each channel and carrier differ from one another concerning their mechanisms and the solute transported. Furthermore, transporter kinetic models aiming to predict transported fluxes typically require knowledge of the kinetic properties of chain reaction steps, such as binding association and dissociation rate constants, transporter turnover rates, and substrate and transporter affinities [19]. An explicit model for the membrane transporter and ion channel of a tissue's cell is unnecessary in most circumstances. Alternatively, when parameters for channels and transporters of one type of cell are unknown, as is often the case, the assumption of using the data of those channels and transporters for other available cells or their isoforms is considered. Therefore, collecting most, if not all, the available models unitedly in one framework can help researchers choose a better fitting model for their

study, more conveniently.

This article is the second of two papers that the authors prepared to summarize the mathematical models used to understand and engineer the membrane carriers' mechanisms. The first article [20] focused on the essential terminology required to understand and model biological transport mechanisms and compile currently available models. The authors developed an inclusive mathematical framework for mass transport mechanism models in different tissue compartments, including cells, capillaries, and gland ducts, with a primary focus on the mechanisms of membrane-mediated transporters such as channels, uniporters, symporters, pumps, and antiporters without emphasizing any specific group of membrane transporters or ion channels [20].

This article intends to complete the developed framework for mathematical models of membrane transporters by focusing on various transport models via specific classes of essential membrane transporters and ion channels. To that end, the present work gathers most of the mathematical models that have been derived to predict the nutrient and ion transport rate by ion channels and membrane transporters. The classifications of the ion channels and membrane transporters for different cell types and phenomena interpretation are addressed. Specifically, it determines the critical assumptions that the models make, all the details necessary for modeling the membrane transporters' mechanisms and presents the conditions by which the models are chosen, which often go unreported. In this work, the provided ion channel models and the electrophysiological models are mostly based on Ohm's Law, mass-action kinetics, and Goldman-Hodgkin equations, and the membrane transporter models (i.e., symporters, antiporters, and pumps) are based on the membrane transporters' kinetic mechanisms. All channels or transporters with more than one model are presented. Depending on the purpose of using the model, one can use the one that bests fits the study. Models are used from various modeling studies, which mainly include epithelial and endothelial cell models.

The two works together, (the first article [20] and the article in hand) aim to create a comprehensive mathematical modeling toolbox for biological transport mechanisms at different levels, which enables researchers to apply the model to different tissues' cells by choosing the model applicable to the desired transporters and channels in a more convenient way. Our purpose is to substantially save the time and resources needed to study the different membrane transport classes

and improve communication between scientists with different backgrounds in the physiology community.

2. Model Construction

Transport across the cell membrane can be mediated via specific groups of integrated membrane proteins known as transporters, including channels (ion channels and water channels), pumps, carrier-mediated proteins (uniporters, symporters, and antiporters), and receptor-mediated transporters. This paper covers the mathematical models of the following known ion channels, pumps, symporters (cotransporters), and antiporters (exchangers) (see Figure 1):

Ion channels: The ion channel section (section 3) includes models for different families of potassium channels, sodium channels, calcium channels, and chloride channels. Potassium channel sections (section 3.1) include models for inward-rectifier potassium channels (IRKC, *Kir*), calcium-activated potassium channels (CaKC), voltage-gated potassium channels (VGPC), ATP-sensitive potassium channels (K_{ATP}) , and two-pore-domain potassium channels (K2P). Sodium channel sections (section 3.2) include the models for *epithelial sodium channels (ENaC)* and *voltage-gated sodium channels (VGSC or Na_v or VONa)*. Calcium channel models are discussed in section 3.3. The family of *L-type voltage-gated calcium channels (L-type)*, *T-type voltage-gated calcium channels (T-type)*, and *store op-*

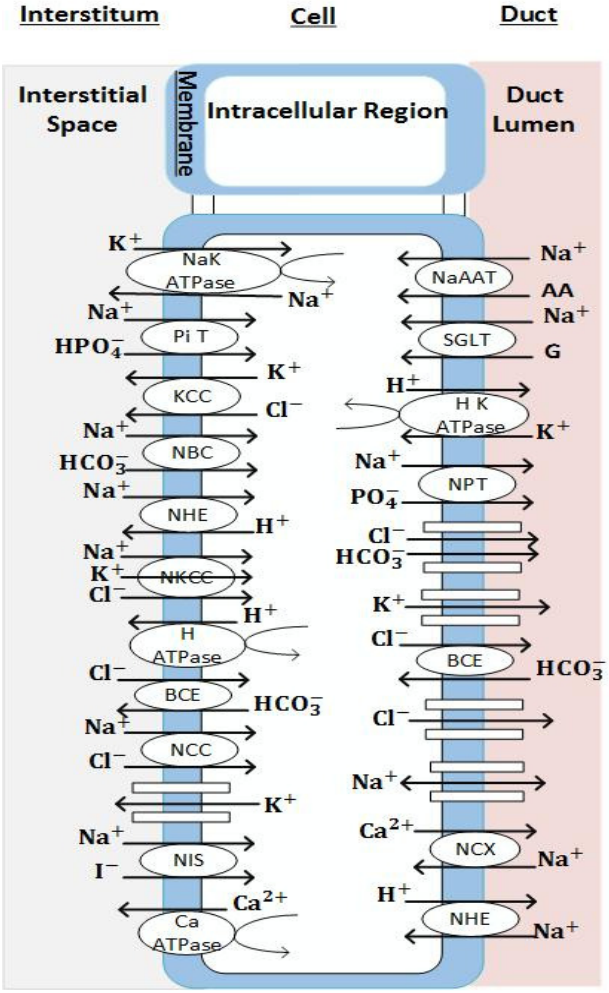

Figure 1: Schematic representation of most of the important transporters and channels across the cell membrane considered in this work.

erated calcium channels (SOC) are included. Finally, chloride channel models, including *cystic fibrosis transmembrane conductance regulator (CFTR)* and *calcium-dependent chloride Channels (CaCC)* groups are are discussed in section 3.4.

ATPase Pumps: The sodium-potassium ATPase pump (Na-K ATPase), (section 4.1), proton ATPase pumps (v-type and H/K ATPase) (section 4.2), and calcium ATPase pump (section 4.4) (PMCA, SERCA) are the three types of ATPase pumps discussed in this work.

Cotrasnporters: Models for cotransporters (symporters) are discussed in section 5. Different mathematical models for sodium-potassium-chloride cotransporter (NKCC) (5.1), potassium chloride cotransporter (KCC) (5.2), sodium chloride cotransporter (NaCl) (section 5.3), sodium bicarbonate cotransporter (NBC) (5.4), sodium phosphate cotransporter (NaPO-4) (5.5), sodium glucose symporter (SGLT) (5.6), and amino acid transporter (5.7) are presented.

Exchangers: Exchangers' (antiporters') section (section 6) includes models for chloride bicarbonate exchanger (BCE) (6.1) [21, 22], sodium calcium exchanger (NCX) (6.2), and sodium hydrogen exchanger (NHE) (6.3).

3. Ion channels

This section includes models to compute the ionic current transferred through the specific types of ion channels, namely, potassium channels (section 3.1), sodium channels (section 3.2), calcium channels (section 3.3), and chloride channels (section 3.4).

3.1. Potassium Channels

Potassium channels are the most diverse ion channel group and play a vital role in regulating the membrane resting potential. Potassium channels are classified based on their selectivity for potassium ions over other ions, the way they are gated, and their conductance properties [23, 24]. There are five major classes of potassium channels: *calcium activated potassium channels* (*CaKC*), *Inward-rectifier potassium channels (K_{ir}, IRK)*, *voltage Gated potassium channel (VGPC)*, *ATP-sensitive potassium channel (KATP)*, and *two-pore-domain potassium channel (leak channels)* [25]. The ionic current through these channels can be obtained using both nonlinear Goldman-Hodgkin-Katz (GHK) and linear Ohm models; depending on the type of potassium

channel and its functionality, one is preferred to the other. In the remaining part of this section, a short discussion of each potassium channel group and its several well-known current models are presented. In all of these models, V_K^{M-N} is the Nernst equilibrium potential of potassium (K) ions and is calculated by eq. (1).

$$V_{K,rev}^{M-N} = \frac{RT}{z_K F} ln\Big(\frac{[K]_{M(out)}}{[K]_{N(in)}}\Big) \tag{1}$$

where F is Faraday's constant (in Coulombs/moles), R is the real gas constant (in J/K moles), T is the absolute temperature (in K), and $[K]_{M(out)}$ and $[K]_{N(in)}$ are the potassium concentration in the extracellular and intracellular regions, respectively.

*3.1.1. **I**nward-**R**ectifier Potassium (**K**) **C**hannels (IRKC, Kir)*

Inward-rectifier potassium channels, also known as *IRKC* or *Kir*, allow the movement of potassium ions more readily into the cell (inward direction) than out of the cell [26, 27]. The current flowing through the individual *IRKC* or *Kir* channels is a function of potassium ion concentration and membrane voltage and is obtained through eq. (2) [28–31].

$$\boxed{i_{K,kir}^{M-N} = g_{kir} f_o^{k,kir} (V_m^{M,N} - V_{K,rev}^{M-N})} \tag{2}$$

where g_{kir} is the cell conductance for potassium ions through Kir channels, $f_o^{k,kir}$ represents the open probability of these channels, V_m^{M-N} is the membrane potential and $V_{K,rev}^{M-N}$ is the Nernst equilibrium potential for potassium ions.

The *Kir* channel conductance, g_{kir}, is a function of potassium ion concentration in the extracellular region (outside the cell) and membrane voltage [28, 32, 33] and can be obtained by eq. (3), where g_{kir}^{max} is a constant [28]. The open probability of the *Kir* channel ($f_o^{k,kir}$) is well described by the Boltzmann relationship, which is shifted leftward by $V_{1/2,kir}$ in mV unit (eq. (4)).

$$g_{kir} = g_{kir}^{max} \left(\frac{[K]_e}{[K]_{ref}}\right)^{n_{kir}} \tag{3}$$

$$f_o^{k,kir} = \frac{1}{1 + exp\left(\frac{V_m^{M-N} - V_{1/2,kir}}{k_{kir}}\right)} \tag{4}$$

where k_{kir} is the inward-rectifier constant (in mV), which is also known as the steepness factor of the conductance-voltage relationship [28], and $V_{1/2,Kir}$ is the half-activation potential (in mV) and function of the intracellular potassium concentration ($[K]_i$). The half-activation potential for Kir channels can be modeled through eq. (5) [31].

$$V_{1/2,kir} = A \log[K]_i + B \tag{5}$$

Here, A and B are constants and determine the voltage shift per decade increase in intracellular potassium concentration

*3.1.2. **C**alcium-**A**ctivated Potassium (**K**) **C**hannels (CaKC)*

Calcium-activated potassium channels, known as $CaKC$s, play an important role in regulating potassium concentration in the cell [34]. These channels are classified based on their conductance level to large conductance (BK or $maxiK$), intermediate conductance (IK), and small conductance (SK). The BK family of $CaKC$s regulates intracellular calcium concentration and membrane voltage, and they prevent a large, sustained depolarization of the cell. BK channels can be activated by membrane depolarization and/or the rise in the intracellular calcium concentration. The SK and IK groups are voltage-sensitive and can be activated by a low level of intracellular calcium concentration [27].

The potassium current through all three groups of calcium-dependent potassium channels (i.e., SK, IK, and BK) can be obtained by eq. (6).

$$\boxed{I''^{M-N}_{K,X_{CaKC}} = n''^{M-N}_{X_{CaKC}}\, g_{X_{CaKC}}\, f_o^{K,X_{CaKC}}\, A\left(V_m^{M-N} - V_{K,rev}^{M-N}\right)} \tag{6}$$

In this equation (eq. (6)), X denotes SK or IK or BK, n''^{M-N}_{CaKC} is the CaKC channel density and represents the number of CaKC channels per unit area of the membrane, g_{CaKC} is the maximum whole-cell conductance for the potassium channels (in nS unit), and $f_o^{K,CaKC}$ is the open probability for CaKC channels [35–37]. The open probability for the CaKC channels ($f_o^{K,CaKC}$) located on the

apical face is modeled by Hill model (eq. (7)).

$$f_o^{K,CaKC} = \frac{1}{1 + \left(\frac{K_{Ca}^{CaKC}}{[Ca]_{i(c)}}\right)^{\eta_{CaKC}}} \tag{7}$$

where η_{CaKC} is the Hill coefficient, K_{Ca}^{CaKC} is the potassium concentration for half-maximumal activation, and $[Ca]_i$ is the intracellular calcium concentration level. IK and BK channels can be activated by low stimuli of the intracellular calcium concentration. Therefore, in some studies, the open probability for the IK and BK channels is considered to be one (i.e., $f_o^{K,CaKC} = 1$) and the current carried through these channels is modeled with Goldman-Hodgkin-Katz equation (eq. (8)) [38].

$$\boxed{I''^{M,N}_{K,X_{CaKC}} = n''_{X_{CaKC}} P^{M-N}_{K,X_{CaKC}} \frac{z_K^2 F^2 V_m^{M-N}}{RT} \frac{[K]_M - [K]_N exp\frac{-z_K F V_m^{M-N}}{RT}}{1 - exp\frac{-z_K F V_m^{M-N}}{RT}}} \tag{8}$$

where X denotes IK or BK, $n''_{X_{CaKC}}$ is the CaKC channel density per unit area of the membrane, $P^{M-N}_{K,X_{CaKC}}$ is the permeability coefficient for the potassium ions through the CaKC channels, and z_K is the ionic charge for potassium ion, $z_K = 1$.

$CaKC$ channels of high conductance (BK) are expressed ubiquitously in smooth muscle tissues, especially in vascular smooth muscle, where the outward current is mainly attributed to the calcium-activated potassium current [39–42]. The current through a single high conductance calcium-activated potassium channel can be obtained through eq. (9).

$$\boxed{i^{M-N}_{K,BK_{CaKC}} = g_{BK_{CaKC}} f_o^{BK_{CaKC}} \left(V_m^{M-N} - V_{K,rev}^{M-N}\right)} \tag{9}$$

In this equation, $f_o^{BK_{CaKC}}$ is the open probability of the CaKC channel and is given by eq. (10). The time-course of channel's open probability consists of fast and slow components. These two components are denoted as $f_f^{BK_{CaKC}}$ and $f_s^{BK_{CaKC}}$ in eq. (10) and are obtained through eqs. (11) and (12). C_f and C_s are the corresponding fast and slow activation constant coefficients (e.g., in Yang

et al.'s model [31]$C_f = 0.65$ and $C_s = 0.35$).

$$f_o^{BK_{CaKC}} = C_f f_f^{BK_{CaKC}} + C_s f_s^{BK_{CaKC}} \tag{10}$$

$$\frac{df_f^{BK_{CaKC}}}{dt} = \frac{\bar{f}_f^{BK_{CaKC}} - f_f^{BK_{CaKC}}}{\tau_{f_f}^{BK_{CaKC}}} \tag{11}$$

$$\frac{df_s^{BK_{CaKC}}}{dt} = \frac{\bar{f}_s^{BK_{CaKC}} - f_s^{BK_{CaKC}}}{\tau_{f_s}^{BK_{CaKC}}} \tag{12}$$

In eqs. (11) and (12), $\tau_{f_f}^{CaKC}$ (ms) and $\tau_{f_s}^{CaKC}$ (ms) are the correspondence mean time constants for the fast and slow open probability, rspectively (e.g., in Yang et al. model [31], $\tau_{f_f}^{BK_{CaKC}} = 0.5ms$ for fast and slow activation gate and $\tau_{f_s}^{BK_{CaKC}} = 11.5ms$). $\bar{f}_o^{BK_{CaKC}}$ represents the steady state open probability of the high conductance CaKC channel. The steady-state open probability of the high conductance calcium-activated potassium channel ($\bar{f}_o^{BK_{CaKC}}$) is voltage-dependent and is described by the Boltzmann relationship that is shifted leftward by $V_{1/2,BK_{CaKC}}$ mV [31] and can be obtained through eq. (13).

$$\bar{f}_o^{BK_{CaKC}} = \frac{1.0}{1.0 + exp[\frac{-(V_m^{M-N} - V_{1/2,BK_{CaKC}}^{M-N})}{k_{CaKC}}]} \tag{13}$$

$$\bar{f}_f^{BK_{CaKC}} = \bar{f}_s^{BK_{CaKC}} - \bar{f}_o^{BK_{CaKC}} \tag{14}$$

where $k_{BK_{CaKC}}$ is the high conductance CaKC channel's constant in the unit of mV and $V_{1/2,BK_{CaKC}}$ is the half-activation potential for the high conductance CaKC channels and can be obtained through eq. (15).

$$V_{1/2,BK_{CaKC}} = A \log[Ca]_i + B \tag{15}$$

where A and B are constants and determine the voltage shift per decade increase in intracellular calcium concentration (e.g., in Yang et al. model [31] $A = -45.0$, $B = 198.55$).

3.1.3. *Voltage Gated Potassium Channel (VGPC, k_v)*

Voltage-gated potassium channels, also known as VGPC or K_v, play a vital role in returning the depolarized cell to a resting state [27]. When the membrane potential becomes less negative or more positive, the VGPC channels limit further membrane depolarization and help repolarize nerve and muscle cells after action potentials [43, 44]. Therefore, this type of voltage-gated family of potassium channels is distinct from "inward" rectifying potassium channels (*IRKC*s), which drive the membrane potential back to the resting potential by impacting the flow of charged potassium ions into the cell. For this reason, they are also known as "delayed rectifier" or "outward rectifying" potassium channels. The potassium current carried through a single VGPC channel can be obtained through eq. (16) [31].

$$\boxed{i_{K,K_v} = g_{K_v}(f_o^{Kv})^2\left(V_m^{M-N} - V_{K,rev}^{M-N}\right)} \tag{16}$$

where g_{K_v} represents the cell conductance for VGPC channels, f_o^{Kv} represents the steady state open probability of the K_v channel and is given by eq. (17).

$$f_o^{Kv} = C_f f_f^{Kv} + C_s f_s^{Kv} \tag{17}$$

In this equation, f_f^{Kv} and f_s^{Kv} denote the fast and slow components of the channel activation process, respectively and are two exponential components of the activation process and C_f and C_s are their correspondence coefficients (e.g., in Yang et al.'s model $C_f = 0.65$ and $C_s = 0.35$) [31]. The fast (f_f^{Kv}) and slow (f_s^{Kv}) components are obtained through eqs. (18) and (19), respectively.

$$\frac{df_f^{Kv}}{dt} = \frac{\bar{f}_o^{Kv} - f_f^{Kv}}{\tau_{f_f}^{Kv}} \tag{18}$$

$$\frac{df_s^{Kv}}{dt} = \frac{\bar{f}_o^{Kv} - f_s^{Kv}}{\tau_{f_s}^{Kv}} \tag{19}$$

where $\tau_{f_f}^{Kv}$ and $\tau_{f_s}^{Kv}$ denote the respective time constants for the fast and slow components of the channel activation process and are obtained through eqs. (20) and (21), respectively.

$$\tau_{f_f}^{Kv} = A_{\tau_{f_f}^{Kv}}\, exp\left[\left(\frac{-(V_m^{M-N} + V_{\tau_{f_f}^{Kv}})}{k_{\tau_{f_f}^{Kv}}}\right)^2\right] - B_{\tau_{f_f}^{Kv}} \tag{20}$$

$$\tau_{f_s}^{Kv} = A_{\tau_{f_s}^{Kv}}\, exp\left[\left(\frac{-(V_m^{M-N} + V_{\tau_{f_s}^{Kv}})}{k_{\tau_{f_s}^{Kv}}}\right)^2\right] + B_{\tau_{f_s}^{Kv}} \tag{21}$$

In these equations, A_{τ_f}, $V_{\tau_f^{Kv}}$, $k_{\tau_f^{Kv}}$, and B_{τ_f} are all constant numbers (e.g., in Yang et al. model [31] for $\tau_{f_f}^{Kv}$ these parameters are defined as: $A_{\tau_{f_f}} = 210.99$, $V_{\tau_f^{Kv}} = 214.34$, $k_{\tau_f^{Kv}} = 195.35$, and $B_{\tau_{f_f}} = -20.59$, and for $\tau_{f_s}^{Kv}$ they are defined as: $\tau_{f_f}^{Kv}$ these parameters are defined as $A_{\tau_{f_s}} = 821.39$, $V_{\tau_s^{Kv}} = 31.59$, $k_{\tau_s^{Kv}} = 27.46$, and $B_{\tau_{f_s}} = 0.19$). Moreover, in eq. (18) $\bar{f}_o^{Kv}$ represents the steady-state open probability of the voltage-gated potassium channels that is voltage-dependent and is described by Boltzmann's relationship that is shifted leftward by $V_{1/2,Kv}$ (in mV unit) [31] and can be obtained through eq. (22).

$$\bar{f}_o^{Kv} = \frac{1.0}{1.0 + exp\left(\frac{-(V_m^{M-N} - V_{1/2,Kv}^{M-N})}{k_{Kv}}\right)} \tag{22}$$

where k_{Kv} is the K_v channel's constant in the unit of mV and $V_{1/2,Kv}$ is the half-activation potential for the K_v channels and can be obtained through eq. (23) [29, 31].

$$V_{1/2,Kv} = A \tag{23}$$

Here A is a constant number and determines the leftward voltage shift (e.g., in Yang et al. model [31] $A = -1.77mV$).

Hodgkin and Huxley [45] developed a mathematical model to find the current through K_v channels from their experimental results in 1990. Their model is given by eq. (24).

$$\boxed{i_{K,Kv} = g_{K_v}\left(V_m - V_{K,rev}\right)} \tag{24}$$

where g_{K_v} represents the cell conductance for VGPC channels (units *conductance*/*area*) and can be obtained by eq. (25).

$$g_{K_v} = g^{\circ}_{Kv} n^4 \tag{25}$$

$$\frac{dn}{dt} = \alpha_n \ \Big(1 - n(t)\Big) - \beta_n \ \ n(t) \tag{26}$$

In eq. (25), g°_{Kv} is a constant for VGPC conductance per unit area of the membrane and n is a dimensionless variable which can vary between 0 and 1. Eq. (26) describes a time course behaviour of the n in which β_n and α_n are rate constants (unit s^{-1}) and they are functions of membrane voltage.

*3.1.4. **ATP**-sensitive Potassium (**K**) Channel (K_{ATP})*

ATP-sensitive potassium channel is gated by the intracellular adenosine triphosphate (ATP) and adenosine diphosphate (ADP) concentration level, where an increase in the ADP/ATP ratio opens K_{ATP} channels [46]. KATP channels are present in a number of tissues, including muscle, pancreatic beta cells and the brain [47–49]. K_{ATP} may also be found on subcellular membranes (e.g., sarcolemmal ("sarcKATP"), mitochondrial ("mitoKATP"), or nuclear ("nucKATP")) [50]. The ionic current through these channels can be obtained through eq. (27) [29, 51].

$$\boxed{I_{K,K_{ATP}} = g_{K_{ATP}} f_o^{K_{ATP}} \Big(V_m^{M-N} - V_{K,rev}^{M-N}\Big)} \tag{27}$$

In this equation, $g_{K_{ATP}}$ is the cell conductance for the K_{ATP} channels which $g_{K_{ATP}}$ depends on extracellular potassium concentration ($[K]_o$) and can be obtained through eq. (28), and $f_o^{K_{ATP}}$ is the open probability for K_{ATP} channels at a given ATP concentration and is modeled by a Hill equation (eq. (29).)

$$g_{KATP} = g_{KATP}^{max} \left(\frac{[K]_o}{[K]_{ref}}\right)^{n_{KATP}} \tag{28}$$

In eq. (28), $[K]_{ref}$ is the reference K concentration and n_{KATP} is a constant number.

$$f_o^{KATP} = \frac{1}{1 + \left(\frac{[ATP]_i}{k_{0.5}}\right)^{\eta_{KATP}}} \tag{29}$$

The K_{ATP} open probability, f_o^{KATP}, can be obtained through eq. (29), where $[ATP]_i$ is the intracellular ATP concentration and $k_{0.5}$ and η_{KATP} are the Hill model parameters. Edwards et al. [29] assumed the ATP concentration remains fixed, and consequently, f_o^{KATP} remains a constant number.

*3.1.5. **T**wo-**P**ore-domain potassium (**K**) channel (K2P)*

Two-pore-domain potassium channels are expressed in both excitable cells (those that can be electrically stimulated, resulting in the creation of electric currents and action potentials such as a neuron and muscle cells) and nonexcitable cells [52, 53]. These channels are always open (i.e., $f_O^{Kleak\ channels} = 1$) and produce baseline (leaky) current across the cell. The current through these channels can be obtained by using Goldman-Hodgkin's model (eq. (30)).

$$I''^{M,N}_{K,leak\ channels} = P^{M-N}_{K,K2P} \frac{z_K^2 F^2 V_m^{M-N}}{RT} \frac{[K]_M - [K]_N exp\frac{-z_K F V_m^{M-N}}{RT}}{1 - exp\frac{-z_K F V_m^{M-N}}{RT}} \tag{30}$$

where $P^{M-N}_{K,K2P}$ is the membrane permeability for potassium ions through a single K2P, $[K]_i$, and $[K]_e$ are the intracellular and extracellular potassium concentrations, respectively [54].

*3.2. Sodium Channels (**NaC**)*

Sodium channels have a high selectivity for sodium ions and play an essential role in regenerating electrical impulses in cardiac muscle, nerve, and skeletal muscle cells [23, 55]. There are two major categories of sodium channels: (i) *epithelial sodium channels (ENaC)* and (ii) *voltage-gated sodium channels (Na_v)*. The ionic current through these channels can be modeled using nonlinear Goldman-Hodgkin-Katz (GHK) and linear Ohm models, depending on the type and functionality of the sodium channel. In the remaining part of this section, a short discussion of each sodium channel group and its ionic current models are presented. In all of these models, V_m^{M-N} is the mem-

brane potential in the unit of mV and V_{Na}^{M-N} is the Nernst equilibrium potential of Na ions which is calculated by eq. (31).

$$V_{Na,rev}^{M-N(a)} = \frac{RT}{z_{Na}F} ln\Big(\frac{[Na]_{M(l)}}{[Na]_{N(i)}}\Big) \tag{31}$$

where F is the Faraday's constant (in Coulombs/moles), R is the real gas constant (in J/K moles), and T is the absolute temperature (in K).

3.2.1. *Epithelial Sodium (**Na**) **C**hannels (ENaC)*

Epithelial sodium channels (ENaC) are located on the apical membrane of epithelial cells in organs, such as distal kidney tubules, lung, respiratory tract, sweat, and salivary glands, and they allow a flow of sodium ions from the extracellular fluid in the lumen into epithelial cells [56, 57]. One way to model the sodium current driven through ENaC channels is by Ohm's equation (eq. (32)).

$$\boxed{I_{ENaC} = n''_{ENaC}\, g_{ENaC} \left(V_m^{M-N} - V_{Na,rev}^{M-N}\right)} \tag{32}$$

where n''_{ENaC} represents density per area of the channel, g_{ENaC} is the membrane conductance for sodium channels, and V_m^{M-N} is the membrane potential in the unit of mV [35, 36]. A second way to describe the sodium current across the cell's membrane is through the Goldman-Hodgkin-Katz model (eq. (33)).

$$\boxed{I_{Na,ENaC}^{M,N} = P_{Na,ENaC}^{M-N} \frac{z_{Na}^2 F^2 V_m^{M-N}}{RT} \frac{[Na]_M - [Na]_N exp\frac{-z_{Na}FV_m^{M-N}}{RT}}{1 - exp\frac{-z_{Na}FV_m^{M-N}}{RT}}} \tag{33}$$

Where $P_{Na,ENaC}^{M-N(a)}$ is the permeability coefficient for the sodium ions through the ENaC channels [25, 38].

3.2.2. *Voltage **G**ated **S**odium **C**hannel (VGSC, Na_v, VONa)*

Voltage-gated sodium channel belong to the family of ion channels that regulate the transmembrane electrical potential. For this reason, they are known as voltage-gated sodium channels [23].

The sodium channels on cell membranes in excitable tissues are mostly from the voltage-gated family of sodium channels. In modeling the gating mechanism of Na_v, some researchers consider a single inactivation gate [29, 58, 59], whereas some have considered two inactivation gates [60–63]. Edwards et al. assume a single activation gate and a single inactivation gate [29]. Under these assumptions, the sodium current carried through a single Na_v channel can be obtained through eq. (34) [29, 58].

$$\boxed{I_{Na,Na_v} = g^{max}_{Na_v} m^3_{Na_v} \; h_{Na_v} \; \left(V_m - V^{M-N}_{Na,rev}\right)} \tag{34}$$

where m_{Na_v} and h_{Na_v} are the activation and inactivation components and are obtained through eqs. (35) and (36), respectively.

$$\frac{dm_{Na_v}}{dt} = \frac{\bar{m}_{Na_v} - m_{Na_v}}{\tau_m} \tag{35}$$

$$\frac{dh_{Na_v}}{dt} = \frac{\bar{h}_{Na_v} - h_{Na_v}}{\tau_h} \tag{36}$$

In eqs. 35 and 36, $\bar{m}_{Na_v}$ and $\bar{h}_{Na_v}$, denote the respective voltage dependent steady-state values and τ_m and τ_h are the associated time constants (e.g., in Edwards's model , based on data obtained through Zhang group, [58] $\tau_m = 0.1(mS)$ and $\tau_h = 1(mS)$). The steady-state activation and inactivation values can be modeled through eqs. (37) and (38), respectively.

$$\bar{m}_{Na_v} = \frac{1}{1 + exp\left(\frac{-(V^{M-N}_m + V^{M-N}_{1/2,m\,Na_v})}{k_{m\,Na_v}}\right)} \tag{37}$$

$$\bar{h}_{Na_v} = \frac{1}{1 + exp\left(\frac{(V^{M-N}_m + V^{M-N}_{1/2,h\,Na_v})}{k_{h\,Na_v}}\right)} \tag{38}$$

where $V_{1/2,m}$ and $V_{1/2,h}$ are the half-activation and half-inactivation voltages for Na_v channels and k_{m,Na_v} and k_{h,Na_v} are the corresponding channel's gating slope in the unit of mV.

Beeler and Reuter [61] proposed a three gated formulation for obtaining the current through

these channels: closed, open, and inactivated [61–63]. Their model is given by eq. (39).

$$\boxed{I_{Na,Na_v} = g^{max}_{Na_v} m^3_{Na_v} h_{Na_v} j_{Na_v} \left(V_m - V^{M-N}_{Na,rev}\right)} \tag{39}$$

where m_{Na_v}, h_{Na_v}, and j_{Na_v} are the activation, inactivation and slow inactivation gates (components) and can be obtained through eqs. (40), (41), and (42), respectively.

$$\frac{dm_{Na_v}}{dt} = \frac{\bar{m}_{Na_v} - m_{Na_v}}{\tau_m} \tag{40}$$

$$\frac{dh_{Na_v}}{dt} = \frac{\bar{h}_{Na_v} - h_{Na_v}}{\tau_h} \tag{41}$$

$$\frac{dj_{Na_v}}{dt} = \frac{\bar{j}_{Na_v} - j_{Na_v}}{\tau_j} \tag{42}$$

In these equations, $\bar{m}_{Na_v}$, $\bar{h}_{Na_v}$, and $\bar{j}_{Na_v}$ are the respective steady-state values for the activation, inactivation, and slow inactivation components and τ_m, τ_h, and τ_j denote the associated time constants. The steady-state values, $\bar{m}_{Na_v}$, $\bar{h}_{Na_v}$, and $\bar{j}_{Na_v}$ can be obtained via eqs. (43), (38), and (45), respectively. The time-constants, τ_m (ms), τ_h (ms),and τ_j (ms), are defined in terms of transition rates through eqs. (46), (47), and (48), respectively.

$$\bar{m}_{Na_v} = \frac{1}{\left(1 + exp\left(\frac{-(V^{M-N}_m - V^{M-N}_{1/2,m\,Na_v})}{k_{m\,Na_v}}\right)\right)^2} \tag{43}$$

$$\bar{h}_{Na_v} = \frac{1}{\left(1 + exp\left(\frac{(V^{M-N}_m + V^{M-N}_{1/2,h\,Na_v})}{k_{h\,Na_v}}\right)\right)^2} \tag{44}$$

$$\bar{j}_{Na_v} = \frac{1}{\left(1 + exp\left(\frac{(V^{M-N}_m + V^{M-N}_{1/2,j\,Na_v})}{k_{j\,Na_v}}\right)\right)^2} \tag{45}$$

$$\tau_m = \alpha_m \beta_m \tag{46}$$

$$\tau_h = \frac{1}{\alpha_h + \beta_h} \tag{47}$$

$$\tau_j = \frac{1}{\alpha_j + \beta_j} \tag{48}$$

In eqs. (46), (47), and (48), α_m, β_m are the activation kinetics and α_h, β_h, α_j, and β_j are the

inactivation kinetics of the associated time constants (τ_m, τ_h, and τ_j). The voltage dependency of transition rates ($\alpha_m, \beta_m, \alpha_h, \beta_h, \alpha_j$, and β_j) are defined using Eyring derived exponential eqs. (49), (50), (51), (52), and (53) [64, 65].

$$For\ all\ range\ of\ V_m : \begin{cases} \alpha_m = \frac{1}{1+exp\left(\frac{-(V_m^{M-N}+V_{1\alpha_m})}{k_{\alpha_m}}\right)} \\ \beta_m = \frac{A_{\beta_m}}{1+exp\left(\frac{(V_m^{M-N}+V_{1\beta_m})}{k_{\beta_m}}\right)} + \frac{B_{\beta_m}}{1+exp\left(\frac{(V_m^{M-N}-V_{2\beta_m})}{k_{2\beta_m}}\right)} \end{cases} \tag{49}$$

$$For\ \ V_m \geq -40 : \begin{cases} \alpha_h = 0 \\ \beta_h = \frac{A_{\beta_h}}{1+exp\left(\frac{-(V_m^{M-N}+V_{1\beta_h})}{k_{\beta_h}}\right)} \end{cases} \tag{50}$$

$$For\ \ V_m < -40 : \begin{cases} \alpha_h = A_{\alpha_h} exp\left(\frac{-(V_m+V_{\alpha_h}^{Na_v})}{k_{\alpha_h}^{Na_v}}\right) \\ \beta_h = A_{\beta_h}\ exp(a_{\beta_h}\ V_m) + B_{\beta_h} exp(b_{\beta_h} V_m) \end{cases} \tag{51}$$

$$For\ \ V_m \geq -40 : \begin{cases} \alpha_j = 0 \\ \beta_j = \frac{A_{\beta_j} exp(-a_{\beta_j}\ V_m)}{1 + exp\left(\frac{-(V_m^{M-N}+V_{2\beta_j})}{k_{\beta_j}}\right)} \end{cases} \tag{52}$$

$$For\ \ V_m < -40 : \begin{cases} \alpha_j = \frac{\left(A_{\alpha_j} exp(a_{\alpha_j} V_m) - B_{\alpha_j} exp(b_{\alpha_j} V_m)\right)(V_m + V_{1\alpha_j})}{1 + exp(\frac{V+V_{2\alpha_j}}{k_{\alpha_j}})} \\ \beta_j = \frac{A_{\beta_j} exp(a_{\beta_j}\ V_m)}{1 + exp\left(\frac{-(V_m^{M-N}+V_{2\beta_j})}{k_{\beta_j}}\right)} \end{cases} \tag{53}$$

In these equations, A_α, A_β, a_α, a_β, B_α, B_β, b_α, b_β, V_α, V_β are all model parameters which can be determined through fitting the ion channel models to the experimental data.

Similarly, Ebihara and Johnson [60] and Luo-Rudy [59] also considered a three gated mechanisms for the Na_v channels. Their models are similar to the three gating mechanism model discussed in eq. (39).

3.3. Calcium Channels

Calcium channels play a critical role in releasing neurotransmitters from the presynaptic neuron into the synaptic cleft. These channels are present in both the plasma membrane and the intracellular organelle membrane. Calcium channels across the plasma membrane create a net calcium flux to the cell, which results in the accumulation of calcium ions in the cytoplasm and functions as a chemical trigger for other cellular mechanisms, such as excitation, secretion of hormones and neurotransmitters, muscle contractions, and adjustment of the gating mechanism of calcium-dependent channels [25, 66–72]. Most of the calcium channels are not always open, and they have gating mechanisms. These channels shift to the open state either due to a change in the voltage across the membrane, *voltage-gated calcium channels (VGCC)*, or through binding a ligand to the channel, *ligand-gated* calcium channels [66, 73].

The voltage-gated calcium channels (VGCCs) are closed at resting membrane potential and become open (activated) by membrane depolarization and allow calcium ion movement into the cytoplasm. VGCCs are slightly permeable to sodium ions (Na^+), and for this reason, they are also known as *Ca-Na channels*. However, in contrast to the NaCa exchanger, which transfers calcium ions out of the cell, these channels contribute to the cytosol's calcium influx [74]. Voltage-gated calcium channels are grouped into different types based on their biophysical and molecular properties. L-type, N-type, P-type, and T-type channels are the four major types of voltage-gated calcium channels identified. L-type calcium channels function in excitation-secretion coupling of endocrine cells and some neurons. N-type calcium channels are restricted to neurons where they function in neurotransmitter release. P-type channels are restricted to Purkinje cells, where they mediate depolarization-induced repetitive spikes. T-type Ca channels, which deactivate more slowly than any other Ca channel, mediate depolarization-induced repetitive spikes in endocrine cells and neurons [73, 75, 76].

There are different types of ligand-gated calcium channels, both on the plasma membrane and intracellular organelle membrane. *store operated calcium channels*, *IP3 receptors*, and *ryanodine receptors* are three significant groups of calcium channels that are activated by ligand binding mechanisms. The store-operated channels are present in the plasma membrane of all of the nonexcitable cells (all cells except myocytes, neurons, and endocrine cells), which cannot be gated by

voltage-gating mechanisms and are gated by a decrease in the calcium concentration level in the the ERSR (two of the intracellular organelles) [68, 77, 78]. SOC channels are studied mostly regarding their role in calcium entry into the cytoplasm from the extracellular milieu. SOCs are permeable to other cations, particularly sodium ions, as well. Consequently, SOC channels are classified as nonselective cation channels due to their different conductance for some other cations [79, 80].

There are two major classes of ligand-gated calcium channels available on the "intracellular organelle's membrane," which release calcium from the intracellular stores (ER, SR, endosomal lysosome) cytoplasm, IP3 receptors, and ryanodine receptors. The underlying mechanism of these ligand-gated calcium channels involves binding the ligand to the channel to turn it into the active form. Thus, in mathematical modeling of these channels, the concentration of corresponding ligands and kinetic terms such as dissociation constant, association constants, binding constants, and unbinding constants should be considered. Due to the complexity involved in their models, these models are not discussed here, and the interested reader is referred to references [81, 82]. More models for ligand-gated calcium channels on the intracellular organelle membrane (e.g., IP3 receptor) can be found in [83, 84]. A review of the existing models of the inositol trisphosphate receptor (IPR) can be found in [29, 83, 85]. The model describing the kinetic mechanism flux across the Ryanodine Receptor (RyR) family of calcium channels can be found in Keizer and Levine's work [86]. Other models of the RyR family can be found in [29, 86, 87].

In this work, the available models to obtain the calcium current through $L-type$, $T-type$, and SOC families of calcium channels are studied. The ionic current through these channels can be obtained using nonlinear Goldman-Hodgkin-Katz (GHK) and linear Ohm model, in which depending on the type of the calcium channel and its functionality, one is preferred to the other. In the remaining part of this section, a short discussion of each group of calcium channels and several well-known current models is presented. In all of these models, V_m^{M-N} is membrane potential (in volts) and $V_{Ca,rev}^{M-N}$ is the Nernst equilibrium potential of calcium ions and is calculated by eq. (54).

$$V_{Ca,rev}^{M-N} = \frac{RT}{z_{Ca}F} ln\Big(\frac{[Ca]_o}{[Ca]_i}\Big) \tag{54}$$

where F is the Faraday's constant (in Coulombs/moles), R is the real gas constant (in J/K moles), and T is the absolute temperature (in K), $[Ca]_o$ is the extracellular concetration of the calcium ions, and $[Ca]_i$ is the intracellular concentration of the calcium ion.

*3.3.1. **L**-type Voltage-Gated **Ca**lcium Channels*

The $L-type$ voltage-gated calcium channels comprise the largest family of membrane VGCCs expressed in various cells, such as skeletal muscle, cardiac cells, ventricular myocytes, smooth muscles, and dendritic cells [88]. The L-type voltage and time-dependent calcium channels can be modeled using the Ohm and nonlinear GHK models.

These channels are highly selective for calcium ions; however, they have a relatively low permeability for sodium and potassium ions [23]. The current through $L-type$ calcium channels can be modeled by the nonlinear Goldman-Hodgkin-Katz (GHK) current equation, which is stated in eq. (55).

$$\boxed{I_i^{Ca_l,M-N} = P_i^M \frac{z_i^2 F^2 V_m^{M-N}}{RT} \frac{\gamma_i^N C_i^N - \gamma_i^M C_i^M exp^{\frac{-z_i FV_m^{M-N}}{RT}}}{1 - exp^{\frac{-z_i FV_m^{M-N}}{RT}}}} \tag{55}$$

$$\boxed{I_{total}^{Ca_l,M-N} = I_{Na}^{Ca_l} + I_{Ca}^{Ca_l} + I_K^{Ca_l}} \tag{56}$$

where $'i'$ refers to any of the ions between calcium ions, sodium ions, and potassium ions. C_i^N and C_i^M are the concentration of the ion 'i' in regions N and M, respectively (in mM), P_i is permeability (in cm/s) of ion 'i', z_i is its valence, γ_i^N, and γ_i^M are the activity coefficient (a.c.) of the ion. The total current through the L-type calcium channel is then obtained through eq. (56) [25, 25, 89, 90].

The voltage-dependency of the L-type calcium channels can be modeled using Ohm equation, as in eq. (57) [29, 31].

$$\boxed{I_{Ca,L} = g_{Ca_L}^{max} f_o^{Ca_l} f_d^{Ca_l} (V_m^{M-N} - V_{Ca,rev}^{M-N})} \tag{57}$$

where $g_{Ca_L}^{max}$ is the maximum cell conductance for calcium L-type channels. The two terms $f_o^{Ca_l}$ and $f_d^{Ca_l}$ represent the activation and inactivation probability of the Ca_L channels, accordingly, which is a dynamic function of the membrane voltage. $f_o^{Ca_l}$ and $f_d^{Ca_l}$ are expressed as in eqs. (58) and (59)

and their multiplication product (i.e., $f_o^{Ca_l} \times f_d^{Ca_l}$) represents the fraction of the Ca_L open channels.

$$f_o^{Ca_l} = C_f f_f^{Ca_l} + C_s \tag{58}$$

$$\frac{df_d^{Ca_l}}{dt} = \frac{\bar{f}_d^{Ca_l} - f_d^{Ca_l}}{\tau_{f_d}^{Ca_l}} \tag{59}$$

$$\frac{df_f^{Ca_l}}{dt} = \frac{\bar{f}_o^{Ca_l} - f_f^{Ca_l}}{\tau_{f_f}^{Ca_l}} \tag{60}$$

In these equations, $\bar{f}_d^{Ca_l}$ and $\bar{f}_o^{Ca_l}$ represent the steady state values of $f_d^{Ca_l}$ and $f_o^{Ca_l}$ and can be obtained through eqs. (61) and (62), respectively. $\tau_{f_d}^{Ca_l}$ and $\tau_{f_f}^{Ca_l}$ denote the respective time constants for activation and inactivation gates, respectively, and they depend on the membrane potential. These time constants, $\tau_{f_d}^{Ca_l}$ and $\tau_{f_f}^{Ca_l}$, can be obtained through eqs. (63) and (64), respectively.

$$\bar{f}_d^{Ca_l} = \frac{1.0}{1.0 + exp\left(\frac{-(V_m^{M-N} + V_{1/2,f_d}^{Ca_l,M-N})}{k_{f_d}^{Ca_l}}\right)} \tag{61}$$

$$\bar{f}_o^{Ca_l} = \frac{1.0}{1.0 + exp\left(\frac{(V_m^{M-N} + V_{1/2,f_o}^{Ca_l,M-N})}{k_{f_o}^{Ca_l}}\right)} \tag{62}$$

$$\tau_{f_d}^{Ca_l} = A_{\tau_{f_d}^{Ca_l}}\, exp\left[\left(\frac{-(V_m + V_{\tau_{f_d}^{Ca_l}})}{k_{\tau_{f_d}^{Ca_l}}}\right)^2\right] + B_{\tau_{f_d}^{Ca_l}} \tag{63}$$

$$\tau_{f_f}^{Ca_l} = A_{\tau_{f_f}^{Ca_l}}\, exp\left[\left(\frac{-(V_m - V_{\tau_{f_f}^{Ca_l}})}{k_{\tau_{f_f}^{Ca_l}}}\right)^2\right] + B_{\tau_{fl}^{Ca_l}} \tag{64}$$

In eqs. (61) and (62), $V_{1/2,f_d}^{Ca_l,M-N}$ and $V_{1/2,f_o}^{Ca_l,M-N}$ are half-activation and half-inactivation potentials for Ca_l channels, which are considered to be constant (i.e., $V_{1/2,f_d}^{Ca_l,M-N} = A_{f_d}^{Ca_l}$ and $V_{1/2,f_o}^{Ca_l,M-N} = A_{f_o}^{Ca_l}$).

3.3.2. *T-type Voltage- Gated Calcium Channels*

The calcium current through the T-type family of the voltage-dependent calcium channels of neurons can be expressed by eq. (65) [91–94].

$$I_{Ca,Ca_t}^{M-N} = \overline{P}_{Ca,CaL}^{M-N} m_{Ca_t}^3 h_{Ca_t} \frac{z_{Ca}^2 F^2 V_m^{M-N}}{RT} \frac{[Ca]_i - [Ca]_o exp\left(\frac{-z_{Ca} F V_m^{M-N}}{RT}\right)}{1 - exp\left(\frac{-z_{Ca} F V_m^{M-N}}{RT}\right)} \tag{65}$$

where $\overline{P}_{Ca,CaL}^{M-N}$ represents the permeability coefficient for the calcium ions through the Ca_L channels and m_{Ca_t} and h_{Ca_t} are the activation and inactivation gating components (parameters) of the Ca_L channels. Huguenard et al. [91] developed a set of empirical equations describing the voltage dependency of each of these gating variables. Their developed equations are given in eqs. (66) and (67).

$$\frac{dm_{Ca_t}}{dt} = \frac{\bar{m}_{Ca_t} - m_{Ca_t}}{\tau_m^{Ca_t}} \tag{66}$$

$$\frac{dh}{dt} = \frac{\bar{h} - h}{\tau_h} \tag{67}$$

$$\bar{m}_{Ca_t} = \frac{1}{1 + exp\left(\frac{-(V_m^{M-N} + V_{1/2,m\ Ca_v}^{M-N})}{k_{m\ Ca_v}}\right)} \tag{68}$$

$$\bar{h}_{Ca_t} = \frac{1}{1 + exp\left(\frac{(V_m^{M-N} + V_{1/2,h\ Ca_t}^{M-N})}{k_{h\ Ca_t}}\right)} \tag{69}$$

In these equations, $\bar{m}_{Ca_t}$ and $\bar{h}_{Ca_t}$ are the respective steady-state values for m_{Ca_t} and h_{Ca_t} gating variables and $\tau_m^{Ca_t}$ and $\tau_h^{Ca_t}$ denote the associated time constants which can be classified and obtained

as below.

$$For\ all\ range\ of\ V_m : \left\{ \tau_m^{Ca_t} = \frac{A_{\tau_m^{Ca_t}}}{exp\left(\frac{-(V_m^{M-N}+V_{1\tau_m})}{k_{1\tau_m}}\right) + exp\left(\frac{(V_m^{M-N}+V_{2\tau_m})}{k_{2\tau_m}}\right)} + B_{\tau_m^{Ca_t}} \right. \tag{70}$$

$$For\ \ V_m \geq -80mV : \left\{ \tau_h^{Ca_t} = A_{\tau_h^{Ca_t}}\ exp\left[\frac{-(V_m + V_{\tau_h^{Ca_t}})}{k_{\tau_h^{Ca_t}}}\right] + B_{\tau_h^{Ca_t}} \right. \tag{71}$$

$$For\ \ V_m < -80mV : \left\{ \tau_h^{Ca_t} = A_{\tau_h^{Ca_t}}\ exp\frac{(V_m + V_{\tau_h^{Ca_t}})}{k_{\tau_h^{Ca_t}}} \right.$$

3.3.3. *Store Operated Channels (SOC)*

Two comprehensive mathematical models describing the calcium and sodium fluxes through SOC channels are presented here: one is the model developed by Edwards et al. [29], and the other is developed by Silva et al. [30]. A general mathematical model representing the calcium current through SOC was developed by Lebeau et al. [69] and formulated by Edwards [29]. Edwards et al. modeled the calcium current by applying the Ohm model (eq. (72)) and then used the nonlinear Goldman-Hodgkin-Katz model in addition to the relative sodium permeability through these channels to relate the sodium current through these channels to that of the calcium current (eq. 73).

$$\boxed{I_{Ca,SOC}^{M-N} = g_{Ca,SOC}^{max} f_o^{SOC} \left(V_m^{M-N} - V_{Ca,rev}^{M-N}\right)} \tag{72}$$

$$\boxed{I_{Na,SOC}^{M-N} = I_{Ca,SOC}^{M-N} \left(\frac{z_{Na}^2 P_{Na}^{SOC}}{z_{Ca}^2 P_{Ca}^{SOC}}\right) \times \left(\frac{[Na]_i - [Na]_o exp\left(\frac{-z_{Na}FV_m^{M-N}}{RT}\right)}{[Ca]_i - [Ca]_o exp\left(\frac{-z_{Ca}FV_m^{M-N}}{RT}\right)}\right)\left(\frac{1 - exp\left(\frac{-z_{Ca}FV_m^{M-N}}{RT}\right)}{1 - exp\left(\frac{-z_{Na}FV_m^{M-N}}{RT}\right)}\right)} \tag{73}$$

Here, $g_{Ca,SOC}^{max}$ is the SOC channel's maximum conductance for calcium ions, and f_o^{SOC} is the open probability of the SOC channels, which can be obtained through eq. (74).

$$f_o^{SOC} = \frac{1}{1 + \frac{[Ca]_{sr}^{\eta_{SOC}}}{K_{SOC}^{\eta_{SOC}}}} \tag{74}$$

where $[Ca]_{sr}$ is the calcium concentration in the ER/SR compartments, η_{SOC} is the Hill coefficient for the SOC channels, and K_{SOC} is the calcium concentration at which the open probability is 50%.

Eq. (74) represents the dependency of the open probability of the SOC channels on the calcium concentration in the ER/SR compartments. Silva et al. [30] obtained calcium and sodium fluxes using the Goldman-Hodgkin-Katz current model through eqs. (75) and (76), respectively.

$$I^{M,N}_{Ca,SOC} = A^{M-N}_{m} P^{M-N(a)}_{Ca,SOC} \frac{z^2_{Ca}\, F^2 V^{M-N}_{m}}{RT} \frac{[Ca]_i - [Ca]_o exp^{\frac{-z_{Ca} F V^{M-N}_{m}}{RT}}}{1 - exp^{\frac{-z_{Ca} F V^{M-N}_{m}}{RT}}} \tag{75}$$

$$I^{M,N}_{Na,SOC} = A^{M-N}_{m} P^{M-N(a)}_{Na,SOC} \frac{z^2_{Na}\, F^2 V^{M-N}_{m}}{RT} \frac{[Na]_i - [Na]_o exp^{\frac{-z_{Na} F V^{M-N}_{m}}{RT}}}{1 - exp^{\frac{-z_{Na} F V^{M-N}_{m}}{RT}}} \tag{76}$$

where $P^{M-N(a)}_{Ca,SOC}$ and $P^{M-N(a)}_{Na,SOC}$ are the apical membrane permeability coefficients for the calcium and sodium ions through SOC channels, respectively. In Silva et al.'s model [30], the calcium permeability through the SOC channels was considered to be constant, and the sodium permeability through these channels was considered to be regulated by the extracellular calcium concentration and calculated through eq. (77).

$$P^{M-N}_{Na,SOC} = \frac{P^{max}_{SOC}}{1 + \left(\frac{[Ca]_o}{K_{SOC,Ca_o}}\right)^{\eta_{SOC,Na}}} \tag{77}$$

The total current through the SOC channel following the Edwards et al. model can be obtained through eq. (78).

$$I^{M,N}_{SOC,total} = f^{SOC}_{o} \left(I^{M,N}_{Ca,SOC} + I^{M,N}_{Na,SOC}\right) \tag{78}$$

where f^{SOC}_{o} is the open probability for SOC channels and is obtained through eq. (79).

$$f^{SOC}_{o} = a \left(\frac{1}{1 + \left(\frac{[Ca]_{sr}}{K_{SOC}}\right)^{\eta_{SOC}}}\right) + b \tag{79}$$

This equation, similar to eq. (74), represents the SOC's activation mechanism due to decreased calcium concentration in the ER/SR compartments. The mathematical framework describing the calcium-binding mechanism by the SOC channel and the calcium fluxes through SOC channels was developed by Kowalsky et al., which is out of the scope of this work, and the interested reader is referred to reference [95].

3.4. Chloride Channels

Chloride channels can be occupied by different ions and have relatively low selectivity for chloride ions [96]. These channels are classified based on the way they are gated, their conductance properties, and their selectivity for chloride ions over the other ions. The cystic fibrosis transmembrane conductance regulator (CFTR) and calcium-dependent chloride channels (CaCC) are two of the most dominant chloride channel families.

In the remaining part of this section, a short discussion of each chloride channel's group and its several well-known current models are presented. In all of these models, V_m^{M-N} is the transmembrane potential (in mV) and V_{Cl}^{M-N} is the Nernest equilibrium potential for the chloride (Cl) ions and is obtained by eq. (80).

$$V_{Cl}^{M-N(a)} = \frac{RT}{z_{Cl}F} ln\left(\frac{[Cl]_{N(l)}}{[Cl]_{M(i)}}\right) \tag{80}$$

where F is the Faraday's constant ($F = 96490\ Coulombs/moles$), R is the real gas constant ($R = 8.315\ J/(mol \cdot K)$), and T is the absolute temperature (in Kelvin), $[Cl]_{M(out)}$ and $[Cl]_{N(in)}$ are the potassium concentration in the extracellular and intracellular regions, respectively.

3.4.1. **Ca**lcium dependent **C**hloride **C**hannels (CaCC)

Calcium-dependent chloride channels, known as $CaCC$s, are present in both excitable cells, such as skeletal muscle, and nonexcitable cells, such as some endocrine cells [96]. CaCC activation and, consequently, the current carried through these channels depend on the intracellular calcium concentration. The current carried by chloride ions through these channels can be estimated using eq. (81).

$$\boxed{I''^{M-N}_{Cl,CaCC} = n''^{M-N}_{CaCC}\, g_{Cl}^{M-N}\, f_o^{Cl,CaCC}(V_m^{M-N} - V_{Cl}^{M-N(a)})} \tag{81}$$

where n''^{M-N}_{CaCC} is the CaCC channel density per membrane area, g_{Cl}^{M-N} is the maximum whole cell conductance (in siemens units) for chloride anions, $f_o^{Cl,CaCC}$ is the open probability of the CaCC channels and is a function of intracellular calcium concentration. The CaCC open probability

functionality can be modeled by using the Hill model [35] in eq. (82).

$$f_o^{Cl,\,CaCC} = \frac{1}{1 + \left(\frac{K_{CaCC}}{[Ca]_i}\right)^{\eta_{CaCC}}} \tag{82}$$

where K_{CaCC} is the Hill parameter for CaCC model and $[Ca]_{M(i)}$ is the intracellular calcium concentration. For some cells such as the acinar cells, the steady state open probability is described by using the Arreola et al. model (1996) [97] and is obtained by eq. (83) [37, 98].

$$f_o^{Cl,\,CaCC} = \frac{1}{1 + K_2\left(\frac{K_1^2}{[Ca]_i^2} + \frac{K_1}{[Ca]_i} + 1\right)} \tag{83}$$

$$K_1 = 234\ exp\left(\frac{-0.13FV_m^{M-N}}{RT}\right),\ K_2 = 0.58exp\left(\frac{-0.24FV_m^{M-N}}{RT}\right)$$

In eq. (83), K_1 and K_2 are the equilibrium constants in the unit of nM and are voltage-dependent.

For some cells, a high positive membrane voltage can enhance the calcium-dependent activation of the CaCC channels, producing outward rectification of the chloride current through the CaCC [99]. Silva et al. [30] modeled this activation dependency by using the Boltzman function as shown in eq. (84). Their model considered two types of open probability: 1) calcium-dependent activation and 2) high positive V_m-enhanced calcium-dependent activation (f CaCC, HPV) [30]. Calcium-dependent activation of CaCCA was modeled by using a Hill function, and high positive Vm-enhanced calcium-dependent activation, which produces outward rectification of I_{CaCC}, was

modeled using a Boltzmann function (eqs. (86), (87), and (88)).

$$f_o^{Cl,\,CaCC} = f_o^{CaCC,\,HPV}\,\frac{1}{1+(\frac{K_{CaCC}}{[Ca]_i})^{\eta_1}} \tag{84}$$

$$\frac{\mathrm{d}f_o^{CaCC,\,HPV}}{\mathrm{d}t} = \frac{\bar{f}_o^{CaCC,\,HPV} - f_o^{CaCC,\,HPV}}{\tau_{CaCC}} \tag{85}$$

$$\bar{f}_o^{CaCC,HPV} = \frac{1}{1+exp\frac{-\left(V_m - V_{half\,max}^{CaCC}\right)}{V_{CaCC}}} \tag{86}$$

$$V_{half\,max}^{CaCC} = \sigma\sqrt{2ln2} + \mu \tag{87}$$

$$\tau_{CaCC}(V_m) = \frac{1}{\sigma\sqrt{2\pi}} exp\left(-\left(\frac{V_m-\mu}{\sqrt{2}\sigma}\right)^2\right) \tag{88}$$

In eq. (84), $\bar{f}_o^{CaCC,\,HPV}$ represents the steady-state open probability of the CaCC channels and is described by Boltzmann's relationship (eq. (86)). τ_{CaCC} is the time constant of the voltage activation and is obtained by fitting the data to a Gaussian function and getting the corresponding constants (i.e., σ and μ in eq. (88)). $V_{half\,max}^{CaCC}$ is the half-maximum for voltage dependency and can be obtained by eq. (87).

*3.4.2. **C**ystic **F**ibrosis **T**ransmembrane conductance **R**egulator (CFTR)*

Cystic fibrosis transmembrane conductance regulator (CFTR) channels provide a pathway for the movement of chloride ions from the cell into the duct lumen [100]. The chloride current through the CFTR channel can be obtained by applying the nonlinear Goldman-Hodgkin-Katz (GHK) model and using eq. (89) [101] .

$$\boxed{I''^{M,N(a)}_{Cl,CFTR} = n''^{M-N(a)}_{CFTR} P^{M(a)}_{Cl,CFTR} \frac{z_{Cl}^2 F^2 V_m^{M-N(a)}}{RT} \frac{[Cl]_N - [Cl]_M exp\frac{z_{Cl}FV_m^{M-N(a)}}{RT}}{1-exp\frac{z_{Cl}FV_m^{M-N(a)}}{RT}}} \tag{89}$$

In this equation, $n''^{M-N(a)}_{CFTR}$ is the CFTR channel density per membrane area, $P^{M-N(a)}_{Cl,CFTR}$ is the permeability coefficient for the CFTR channel, and $V_m^{M-N(a)}$ is the apical membrane potential in the unit of mV. A second way to obtain the chloride current through CFTR channels is through Ohm's

model (eq. (90)) [38].

$$\boxed{I''^{M-N(a)}_{Cl,CFTR} = n''^{M-N(a)}_{CFTR} g^{M-N}_{CFTR} f_o^{Cl,CFTR}(V_m^{M-N(a)} - V^{M-N(a)}_{Cl,rev})} \tag{90}$$

where $f_o^{Cl,CFTR}$ is the open probability of the CFTR channel and can hold the constant number at rest potential [35, 102]. CFTR channels have a selectivity filter that favors the permeation of chloride ions over other ions. However, they are also relatively permeable to bicarbonate anions. One general approach to consider the selectivity filter of CFTR channels to bicarbonate anions in the CFTR current models is to find the permeation ratio of CFTR channels for bicarbonate anions relative to that for chloride anions [36, 103]. The Ohmic model can then be applied to obtain the chloride and bicarbonate currents through the CFTR channels through eqs. (92) and (91), respectively [36].

$$\boxed{I''^{M-N(a)}_{Cl,CFTR} = n''^{M-N}_{CFTR}\, g_{CFTR} \left(V_m^{M-N} - V^{M-N}_{Cl,rev}\right)} \tag{91}$$

$$\boxed{I''^{M-N(a)}_{HCO3,CFTR} = n''^{M-N}_{CFTR}\, \beta\, g_{CFTR} \left(V_m^{M-N} - V^{M-N}_{HCO3,rev}\right)} \tag{92}$$

In these equations, β represents the ratio of the membrane conductance through the CFTR channel for bicarbonate ions relative to the chloride anions (eq. (93)), n''^{M-N}_{CFTR} is the CFTR channel density per membrane area, and g_{CFTR} is the (membrane) conductance for CFTR channel.

$$\beta = \frac{g_{CFTR,HCO_3}}{g_{CFTR,Cl}} \tag{93}$$

Whitcomb et al. [103] used the effective permeability ($g_x^{i-o}([x]_{Mori}, [x]_{Noro})$) for the CFTR channels to obtain the effective conductance of the cell to each of the ions based on their concentrations. Here, $[X]_i$ and $[X]_o$ refers to concentrations of chloride or bicarbonate anions, inside (i) and outside (o) the cell, respectively. They expressed the chloride and bicarbonate current fluxes by applying

the Ohmic model through eqs. (94) and (95), respectively.

$$\boxed{I''^{M-N}_{Cl,CFTR} = n''^{M-N}_{CFTR}(\bar{g}^{M-N}_{Cl}\ g^{CFTR}_{Cl})\left(V^{M-N(a)}_{m} - V^{M-N}_{Cl,rev}\right)} \tag{94}$$

$$\boxed{I''^{M-N}_{HCO_3,CFTR} = n''^{M-N}_{CFTR}(\bar{g}^{M-N}_{HCO_3}\ g^{CFTR}_{HCO3})\left(V^{M-N(a)}_{m} - V^{M-N}_{HCO_3,rev}\right)} \tag{95}$$

where $g^{M-N}_{x}([x]_M, [x]_N)$ is the effective permeability and can be obtained through eq. (96).

$$g^{M-N}_{x}([x]_M, [x]_N) = [x]_M[x]_N \frac{ln\left(\frac{[x]_M}{[x]_N}\right)}{[x]_M - [x]_N} \tag{96}$$

Further, the Nernst potential for Chloride ions, $V^{M-N}_{Cl,rev}$, and bicarbonate ions, $V^{M-N}_{HCO_3,rev}$, can be obtained through eqs. (97), and (98), respectively.

$$V^{M-N(a)}_{Cl,rev} = \frac{RT}{z_{Cl}F} ln\left(\frac{[Cl]_{N(l)}}{[Cl]_{M(i)}}\right) \tag{97}$$

$$V^{M-N}_{HCO_3,rev} = \frac{RT}{z_{HCO_3}F} ln\left(\frac{[HCO_3]_N}{[HCO_3]_M}\right) \tag{98}$$

where F is the Faraday's constant (in Coulombs/moles), R is the real gas constant (in J/K moles), and T is the absolute temperature (in K).

4. ATPase model

This section includes several kinetic models of ATPase pumps, namely, sodium potassium ATPase pump (section 4.1), proton-ATPase pump (4.2), hydrogen-potassium ATPase pumps (section 4.2), and calcium-ATPase pumps (4.4).

4.1. Sodium Potassium ATPase pump (Na-K ATPase)

Sodium-potassium ATPase (Na-K ATPase) pumps are electrogenic pumps that are essential for maintaining the intracellular concentration of sodium and potassium ions at the desired cellular level, maintaining the membrane potential, and regulating the cell volume, which prevents the cell from lysis [104]. NaK ATPase pumps hydrolysis the ATP molecules to actively transport Na^+ ions out of the cell and K^+ ions into the cell. Reaction eq. (99) summarizes the overall transport

reaction mechanism. In each cycle (one turnover of the pump), three sodium ions exit the cell, while two potassium ions enter the cell [105].

$$\mathrm{ATP} + 3\,\mathrm{Na_M}^{+} + 2\,\mathrm{K_N}^{+} \rightleftharpoons \mathrm{ADP} + \mathrm{Pi} + 3\,\mathrm{Na_N}^{+} + 2\,\mathrm{K_M}^{+} \tag{99}$$

The flux transported by NaKATPase can be obtained by using a Hill-type equation [106]. Eqs. (54a) and (54b) in [20] can be used to model the transported flux. The sodium and potassium fluxes across the pump are expressed by using eqs. (100) and (101).

$$\boxed{J_{Na^+}^{NakATpase} = J_{Na^+}^{NakATpase,max}\Big(\frac{[Na]_{M(i)}}{[Na]_{M(i)} + K_{Na_M}}\Big)^3\Big(\frac{[K]_{N(e)}}{[K]_{N(e)} + K_{K_N}}\Big)^2} \tag{100}$$

$$\boxed{J_{K^+}^{NakATpase} = (\frac{-2}{3})J_{Na^+}^{NakATpase}} \tag{101}$$

where $J_{Na^+}^{NakATpase}$ is the maximum steady-state efflux of the sodium ions and is the function of membrane potential. K_{Na}^{NaK} and K_{K}^{NaK} are the saturation constants for the intracellular sodium (mM) and the extracellular potassium ions, accordingly [22]. K_{Nai} and K_{Ki} are the pump affinity for sodium and potassium ions and can be obtained through eqs. (102) and (103), respectively [106–110].

$$K_{Nai} = K_{Na}^{NaK}(1 + \frac{[K]_i}{a_{NaK}}) \tag{102}$$

$$K_{Ki} = K_{K}^{NaK}(1 + \frac{[Na]_e}{b_{NaK}}) \tag{103}$$

where a_{NaK} and b_{NaK} are the constants are constants that depend on the types of cells each can take different values.

Ammonium (NH_4) competes with potassium ions for the same binding site. Therefore, in the presence of ammonium (NH4) eq. (101) changes to eq. (105), and the ammonium and potassium relative affinity regulates the relation between the transported fluxes of potassium and ammonium

through the eq. (106) [111, 112].

$$J_{Na}^{Pump} = J_{Na}^{NaKATPase,max}\left(\frac{[Na]_c}{[Na]_c + K_{Na}}\right)^3\left(\frac{[K]_{bl}}{[K]_{bl} + K_K}\right)^2 \tag{104}$$

$$J_K^{pump} + J_{NH4}^{pump} = -\frac{2}{3}J_{Na}^{pump} \tag{105}$$

$$\frac{J_{NH4}^{pump}}{J_K^{pump}} = \frac{[NH4]_e}{K_{NH4}} \cdot \frac{K_K}{[K]_e} \tag{106}$$

Luo et al. [113] evaluated the voltage dependency of the current through NaKATPase pumps (I_{NaK}) at different levels of sodium concentration at the extracellular region ([Na]o) and modeled this voltage dependency for cardiac ventricular tissue through eq. (107) [29, 113].

$$I_{NaK}^{M-N} = I_{NaK}^{max}\psi_{NaK}^{cyt}\left(\frac{[Na]_{cyt}^{1.5}}{[Na]_{cyt}^{1.5} + K_{m,Na,\alpha 1}^{1.5}}\right)\left(\frac{[K]_{out}}{[K]_{out} + K_{m,K}}\right) \tag{107}$$

$$\psi_{NaK}^{cyt} = \frac{1}{1 + 0.1245exp\left(-0.1\frac{V_m^{M-N}F}{RT}\right) + 0.365\ \sigma\ exp\left(\frac{-V_m^{M-N}F}{RT}\right)} \tag{108a}$$

$$\sigma = \frac{1}{7}\left(\frac{[Na]_{out}}{67.3} - 1\right) \tag{108b}$$

In this equation, I_{NaK}^{max} is the maximum NaK ATPase current in ($\mu A \mu F^{-1}$) unit and ψ_{NaK}^{cyt} captures the membrane voltage influence on I_{NaK} and is a function of the extracellular sodium concentration on the current produced by NaK ATPase pumps and can be obtained through eq. (108a) in combination with eq. (108b). $K_{m,K}$ is the potassium ($[K]$) half-saturation constant (in mM) for NaK ATPase, and $K_{m,Na,}$ is sodium ($[Na]$) half-saturation constant for NaK ATPase in mM units.

Hartman et al. [38] also included a weak dependence of the NaKATPase turnover rate on basolateral membrane potential [22, 38]. Their model is given by eq. (109).

$$J_{pump} = P_{pump}\left(\frac{[Na]_c}{[Na]_c + K_{Na}}\right)^3\left(\frac{[K]_{bl}}{[K]_{bl} + K_K}\right)^2 (a \times V_m^b + b) \tag{109}$$

Here, $'a \times V_m(b) + b'$ represents the effect of membrane voltage on the current carried by NaK

ATPase pumps, in which 'a' (in the unit of $(mV)^{-1}$) and 'b' (no unit) are constants and when the membrane is at steady-state reduced membrane potential, this voltage correction term is equal to 1 (i.e., $a \times V_m(b) + b = 1$), and P_{pump} is the membrane permeability coefficient in the unit of $\mu mol \cdot cm^{-2} \cdot h^{-1}$.

Sohma et al. [22] developed a simplified model for describing the transported flux by NaKATPase pump (eq. (110)) based on the reparametrization of the Hartman and Hoffman [38, 108] models.

$$J_{NaKATPase} = P_{pump}\left(\frac{[Na]_i}{[Na]_i + K_{Na}^{NaK}}\right)^3\left(\frac{[K]_{bl}}{[K]_{bl} + K_K^{NaK}}\right)^2 (V_m^{i-bl} - V_{rev}) \tag{110}$$

Moreover, Smith and Crampin [114] mathematically described the detailed kinetic mechanism of transport through the NaK ATPase pump, which is out of the scope of this work, and the interested reader is referred to [114].

4.2. Proton-ATPase (H-ATPase)

ATP-driven proton pumps actively transport hydrogen ions across the cell membrane through hydrolysis of adrenalin triphosphate (ATP) molecules. These pumps are classified based on their conformational structure into three groups: *V-type*, *P-type*, and *F-type*. Here, a short discussion of several well-known proton pump current and flux models are presented. In some of these models, the contribution of electrical and chemical components (electrochemical potential dependency) is considered.

Andersen et al. experimentally found a dependency between the hydrogen flux and the electrochemical potential difference across the membrane [115]. This electrochemical potential density is considered in eqs. (111) and (112). Eq. (111) represents the model to obtain the flux of protons due to the proton pump located on an "apical" membrane and eq. (112) represents the equivalent model for the case in which the pump is located on the "basolateral" membrane [109].

$$J_{H,HATPase}^{M-N(a)} = -J_{H,HATPase}^{max}\frac{1}{1 + exp\left(\zeta(\nu_H^{M-N(a)} - \nu_{1/2,H-ATPase}^{M-N(a)})\right)} \tag{111}$$

$$J_{H,HATPase}^{M-N(b)} = J_{H,HATPase}^{max}\frac{1}{1 + exp\left(-\zeta(\nu_H^{M-N(b)} - \nu_{1/2,H-ATPase}^{M-N(b)})\right)} \tag{112}$$

In these equations, $J^{max}_{H,HATPase}$ is the maximum hydrogen flux (i.e., the flux of the ion at saturation) through $H-ATPase$ pumps, $V^{M-N}_{1/2,H-ATPase}$ is the electrochemical potential difference where the flux is half of its maximum value, ζ is the coefficient representing the steepness of the function, v^{M-N}_{H} is the electrochemical potential difference of hydrogen from the M (cytosol) region to the N (luminal) region. The hydrogen flux driven through proton pumps can also be obtained by applying the Hill model (eq. (113)).

$$J^{M(i)-N(e)}_{H,H-ATPase} = J^{max}_{H,HATPase} \frac{[H^+]_{M(cell)}}{K^{M(cell)}_{H,H-ATPase} + [H^+]_{M(cell)}} \tag{113}$$

where $J^{max}_{H,HATPase}$ is the maximum hydrogen flux through $H-ATPase$ pumps and $K_{H,H-ATPase}$ is the affinity of the pump to the H^+ ion [107].

4.3. Hydrogen-Potassium ATPase (H/KATPase)

Nadal et al. [116] developed a nongastric H-K ATPase model based on Weinstein's schematic kinetic diagram, which includes competition between the NH^+_4 and Na^+ ions with hydrogen and potassium ions, respectively. Following Nadal et al.'s model, the net transported flux for sodium, potassium, hydrogen, and ammonia from the cytosol region to the luminal (l or N) region, can be obtained through eqs. (114), (115), (116), and (117), respectively [116].

$$J^{net}_{Na,HK-ATPase} = k^{lc}_{Na}[P_iNa]_l - k^{cl}_{Na}[P_iNa]_c \tag{114}$$

$$J^{net}_{K,HK-ATPase} = k^{lc}_{K}[K]_l - k^{cl}_{K}[K]_c \tag{115}$$

$$J^{net}_{H,HK-ATPase} = k^{lc}_{H}[P_iH]_l - k^{cl}_{H}[P_iH]_c \tag{116}$$

$$J^{net}_{NH4,HK-ATPase} = k^{lc}_{NH4}[NH4]_l - k^{cl}_{NH4}[NH4]_c \tag{117}$$

In these equations, (eqs. (114), (115), (116), and (117)) k^{lc}_X and k^{cl}_X are the translocation rate constants with X bound from the lumen to the cytosol and the cytosol to the lumen (where X is Na^+, K^+, H^+, or $NH4^+$), respectively. $[X]^l$ and $[X]^c$ are the densities of the luminal and cytosolic facing enzymes, respectively, with X bound (where X is $[P_iNa]$, $[K]$, $[P_iH]$, or $[NH4]$). Moreover, in

these equations, the flux is taken positive from the lumen to the cytosol direction.

4.4. Calcium ATPase pumps (Ca − ATPase):

*4.4.1. **P**lasma **M**embrane **C**alcium **A**TPase (**PMCA**):*

Plasma membrane calcium ATPase pumps, also known as *PMCA*, in addition to the sodium-calcium exchanger, are responsible for the cell's calcium ion efflux. PMCA's function is vital for regulating the amount of calcium in the cells, as it has a direct impact on the other channels' mechanisms and cellular mechanisms [117–120]. The energy required to eject calcium ions from the cell through PMCA pumps is supplied through ATP molecule hydrolysis. Because of this enzymatic manner, the calcium flux and the equivalent current through this pump are modeled using the Michaelis-Menten equation, which leads to eqs. (118), and (119), respectively [30, 37, 89, 98, 120, 121].

$$\boxed{I_{PMCA} = I_{PMCA}^{max} \frac{1}{1 + \left(\frac{K_{PMCA,Ca_i}}{[Ca]_{M(i)}}\right)^{\eta_{PMCA}}}} \tag{118}$$

$$\boxed{J_{PMCA}^{M(i)-N(e)} = -\frac{I_{PMCA}}{z_{Ca}F} = \frac{V_{PMCA}[Ca]_{M(i)}^{\eta_{PMCA}}}{K_{PMCA,Ca_i}^{\eta_{PMCA}} + [Ca]_{M(i)}^{\eta_{PMCA}}}} \tag{119}$$

In equations 118 and 119, η_{PMCA} is the Hill coefficient of the pump and Km is the calcium concentration at which the maximum pump current is delivered. Furthermore, the negative sign in eq. (119) shows the calcium flux direction to be out of the cell. More information on detailed kinetic studies of this family of pumps can be found in [122, 123].

*4.4.2. **S**acro **E**ndoplasmic **R**eticulum **C**alcium **A**TPase (**SERCA**):*

SERCA is a family of sar-coplasmic reticulum (SR) calcium pumps that actively transport calcium ions into the SR against their electrochemical gradients to control calcium ion elevation in the cytoplasm region. Different mathematical models have been developed over the years to obtain the calcium ion flux through these pumps. These models can be classified as unidirectional models and bidirectional models.

Here, a unidirectional model for the movement of calcium ions from the cell cytoplasm to

the SERCA is represented. Some models that consider bidirectional movements can be found in [124, 125].

The unidirectional transported flux of calcium through SERCA is mostly modeled by using the Hill equation (eq. (120)) [30, 31, 37, 98, 113, 125, 126].

$$I_{SERCA} = I_{SERCA}^{max} \frac{1}{1 + \left(\frac{K_{SERCA}}{[Ca]_{M(cyt)}}\right)^{\eta_{SERCA}}} \tag{120}$$

where I_{SERCA}^{max} is the maximum current through the pump and η_{SERCA} is the Hill coefficient (mostly considered to be $\eta_{SERCA} = 1$ or $\eta_{SERCA} = 2$ [30, 31, 37, 98, 113, 125, 126]).

The transported calcium flux models through SERCA pumps can become slightly more complicated, as experimental evidence indicates that the SERCA pumping rate is accentuated by calcium concentration outside the SR in the endoplasmic reticulum (ER) [127]. Sneyd et al. modeled this extracellular calcium dependency and represented the flux through the SERCA pump by eq. (121) [125, 128].

$$J_{SERCA} = J_{SERCA}^{max} \frac{(1)}{1 + (\frac{[Ca]_i}{K_{SERCA}})^{\eta_{serca}}} \quad \frac{1}{[Ca]_{er}} \tag{121}$$

where $[Ca]_{er}$ is the calcium concentration in the endoplasmic reticulum (ER) region [128]. Shanon et al. [129] fit the SR calcium uptake data to a second term equation that accounts for back flux and leak current. Their developed model is given in eq. (122).

$$J_{SERCA} = \frac{V_{maxf}\left(\frac{[Ca]_i}{K_{mf}}\right)^{\eta_f} - V_{maxr}\left(\frac{[Ca]_{sr}}{K_{mr}}\right)^{\eta_r}}{1 + \left(\frac{[Ca]_i}{K_{mf}}\right)^{\eta_f} + \left(\frac{[Ca]_{sr}}{K_{mr}}\right)^{\eta_r}} + K([Ca]_{sr} - [Ca]_i) \tag{122}$$

where V_{maxf}, K_{mf}, and η_f are the Hill parameters for the forward pump flux and V_{maxr}, K_{mr}, and η_r are the same parameters for backward pump flux. Moreover, the product $K([Ca]_{sr} - [Ca]_i)$ represents the leak portion of the flux.

Shannon et al. took the similarity assumption for V_{max} and η values for forward and backward pump fluxes in eq. (122) and considered zero to be the leak current. Their model is given by eq.

(123) [29, 90].

$$I_{SERCA} = I_{SERCA}^{max} \frac{\left(\frac{[Ca]_i}{K_{mf}}\right)^{\eta_{serca}} - \left(\frac{[Ca]_{sr}}{K_{mr}}\right)^{\eta_{serca}}}{1 + \left(\frac{[Ca]_i}{K_{mf}}\right)^{\eta_{serca}} + \left(\frac{[Ca]_{sr}}{K_{mr}}\right)^{\eta_{serca}}} \tag{123}$$

5. Cotransporters

This section includes several kinetic models of the important cotransporters (or symporters), namely, sodium-potassium-chloride cotransporter (section 5.1), potassium chloride cotransporter (5.2), sodium chloride cotransporter (section 5.3), sodium bicarbonate cotransporter 5.4, sodium phosphate cotransporter (section 5.5), sodium glucose symporter (section 5.6), and amino acid symporter (5.7).

5.1. Sodium Potassium Chloride Symporter (NKCC):

Sodium-potassium-chloride cotransporter ($Na^+ - K^+ - Cl^-$ cotransporter or NKCC) is a member of the cation-chloride cotransporter family, whose function is regulated by extracellular concentrations of sodium (Na) and potassium (K) ions and intracellular chloride anions (Cl) [130]. Structural analysis of the NKCC transporter kinetic mechanism has led to the construction of several kinetic models for the transport mechanism by members of the NKCC family. Two isoforms of the NKCC protein are currently known. One isoform is NKCC2, which is found exclusively in the kidney, and the other is NKCC1, which is found in nearly all cell types. More details about these isoform structures and their role in the regulation of cellular functions under physiological and pathophysiological conditions can be found in [131–135].

Lytle et al. [136, 137] developed a quantitative transport model for NKCC1, which follows a "first on last off" binding order. In the first step, the carrier faces the extracellular side of the membrane (M or o) and binds to chloride ions (Cl). After the complex ECl_M is formed, a sodium ion (Na) binds to ECl_M and forms the $EClNa_M$ complex, followed by the binding of a second Cl ion to form complex $EClNaCl_M$. Finally, potassium ions (K ions) bind to the transporter to give the fully loaded carrier complex $EClNaClK_M$. In this model, the carriers can translocate across the membrane in all states (i.e., in the empty, partially loaded, and fully loaded states), and the unbinding reactions occur in the reverse order of binding [136–138]. Lytle et al.'s model was

reparametrized and schematically shown in Figure 14a in [20]. Under combined equilibrium and steady-state assumptions, the chloride, sodium, and potassium fluxes can be obtained through eqs. (124a), (124b), and (124c), respectively.

$$J^{M,N(net)}_{Cl,NKCC} = [E]_{NKCC} \left(\frac{R_{NN}\left(g^{M}_{ECl}Cl^{M} + g^{M}_{EClNa}Cl^{M}Na^{M} + g^{M}_{EClNaCl}Cl^{M}Na^{M}Cl''^{M} + g^{M}_{EClNaClK}Cl^{M}Na^{M}Cl''^{M}K^{M}\right)}{R_M R_{NN} + R_N R_{MM}} - \frac{R_{MM}\left(g^{N}_{ECl}Cl^{N} + g^{N}_{EClNa}Cl^{N}Na^{N} + g^{N}_{EClNaCl}Cl^{N}Na^{N}Cl''^{N} + g^{N}_{EClNaClK}Cl^{N}Na^{N}Cl''^{N}K^{N}\right)}{R_M R_{NN} + R_N R_{MM}} \right) \tag{124a}$$

$$J^{M,N(net)}_{Na,NKCC} = [E]_{NKCC} \left(\frac{R_{NN}\left(g^{M}_{EClNa}Cl^{M}Na^{M} + g^{M}_{EClNaCl}Cl^{M}Na^{M}Cl''^{M} + g^{M}_{EClNaClK}Cl^{M}Na^{M}Cl''^{M}K^{M}\right)}{R_M R_{NN} + R_N R_{MM}} - \frac{R_{MM}\left(g^{N}_{EClNa}Cl^{N}Na^{N} + g^{N}_{EClNaCl}Cl^{N}Na^{N}Cl''^{N} + g^{N}_{EClNaClK}Cl^{N}Na^{N}Cl''^{N}K^{M}\right)}{R_M R_{NN} + R_N R_{MM}} \right) \tag{124b}$$

$$J^{M,N(net)}_{K,NKCC} = [E]_{NKCC} \left(\frac{R_{NN}(g^{M}_{EClNaClK}Cl^{M}Na^{M}Cl''^{M}K^{M}) - R_{MM}(g^{N}_{EClNaClK}Cl^{N}Na^{N}Cl''^{N}K^{N})}{R_M R_{NN} + R_N R_{MM}} \right) \tag{124c}$$

where $[E]_t = [E]_M + [ECl]_M + [EClNa]_M + [EClNaCl]_M + [EClNaClK]_M + [EClNaClK]_N + [EClNaCl]_N + [EClNa]_N + [ECl]_N + [E]_N$

K_{ion} is the equilibrium constant of the ion in the unit of *mmol* and the normalized concentrations are:

$Cl^M = \frac{[Cl]_M}{K^M_{Cl}}$, $Na^M = \frac{[Na]_M}{K^M_{ClNa}}$, $Cl''^M = \frac{[Cl]_M}{K^M_{ClNaCl}}$, $K^M = \frac{[K]_M}{K^M_{ClNaClK}}$

$Cl^N = \frac{[A]_N}{K^N_A}$, $Na^N = \frac{[B]_N}{K^N_{ClNa}}$, $Cl''^N = \frac{[A]_N}{K^N_{ABA}}$, $K^N = \frac{[C]_N}{K^N_{ClNaClK}}$

$R_M = 1 + Cl^M + Cl^M Na^M + Cl^M Na^M Cl''^M + Cl^M Na^M Cl''^M K^M$

$R_N = 1 + Cl^N + Cl^N Na^N + Cl^N Na^N Cl''^N + Cl^N Na^N Cl''^N K^N$

$R_{MM} = g^M_E + g^M_{ECl}Cl^M + g^M_{EClNa}Cl^M Na^M + g^M_{EABA}Cl^M Na^M Cl''^M + g^M_{EClNaClK}Cl^M Na^M Cl''^M K^M$

$R_{NN} = g^N_E + g^N_{ECl}Cl^N + g^N_{EClNa}Cl^N Na^N + g^N_{EClNaCl}Cl^N Na^N Cl''^N + g^N_{EClNaClK}Cl^N Na^N Cl''^N K^N$

A different quantitative model of the transported ionic flux due to the NKCC transporter was developed by Benjamin et al. in 1997 [139]. Their model has been widely used in modeling the NKCC transporter in the secretory epithelial cell family, which has NKCC1 in the basolateral face.

Benjamin et al. [139] considered the symmetric order of binding and unbinding (first-on first-off) with a different binding/unbinding order mechanism. In their model, the order of binding is as follows: first, the Na ion binds to the carrier on surface M of the membrane to form the complex ENa_M then the first Cl ion binds to ENa_M and forms the complex $ENaCl_M$. This binding is followed by the binding of K ions and the formation of the complex $ENaClK_M$ complex. In the last binding step, the second Cl ion is bound, and the full complex $ENaClKCl_M$ is formed on the M face of the membrane. In this model, the partially loaded carriers are not capable of translocating, and only the fully bounded and free (unbounded) transporters are considered to be able to cross the membrane. After the translocation of the fully loaded complex to the other side of the membrane, unbinding occurs in symmetric order to the binding order, that is, Na^+ unbinds first, next Cl^- ion is unbound, followed by unbinding of K+ ion, and finally, the second Cl^- unbinds from the complex [98, 131, 137, 140].

Their model contains about 30 terms, which is reparameterized in the equivalent model of Figure 15 in [20]. The steady-state turn over rate of the NKCC cotransporter is given by eq. (125a), and the corresponding fluxes for Na, Cl, and K can be obtained through eqs. (125b), (125c), and (125d), respectively.

$$\boxed{J^{M,N(net)}_{symporter} = [E]_t\left(\frac{\left(g^M_{ENaClKCl}Na^M Cl^M K^M Cl''^M\right)g^N_E - \left(g^N_{ENaClKCl}Na^N Cl^N K^N Cl''^N\right)g^M_E}{R_M R_{NN} + R_N R_{MM}}\right)} \tag{125a}$$

$$\boxed{J^{M,N(net)}_{Na,symporter} = J^{M,N(net)}_{symporter}} \tag{125b}$$

$$\boxed{J^{M,N(net)}_{Cl,symporter} = 2J^{M,N(net)}_{symporter}} \tag{125c}$$

$$\boxed{J^{M,N(net)}_{K,symporter} = J^{M,N(net)}_{symporter}} \tag{125d}$$

where $[E]_t = [E]_M + [ENa]_M + [ENaCl]_M + [ENaClK]_M + [ENaClKCl]_M + [ENaClKCl]_N + [ENaClK]_N + [ENaCl]_N + [ENa]_N + [E]_N$.

K_{ion} is the equilibrium constant of the ion in the unit of *mmol* and the normalized concentrations are:

$Na^M = \frac{[Na]_M}{K^M_{Na}}$, $Cl^M = \frac{[Cl]_M}{K^M_{NaCl}}$, $K^M = \frac{[K]_M}{K^M_{NaClK}}$, $Cl''^M = \frac{[Cl]_M}{K^M_{NaClKCl}}$,

$Na^N = \frac{[Na]_N}{K^N_{NaClKCl}}$, $Cl^N = \frac{[Cl]_N}{K^N_{BCB}}$ $K^N = \frac{[K]_N}{K^N_{ABC}}$, $Na''^N = \frac{[Cl]_N}{K^N_{NaClKCl}}$.

The resistance parameters are defined as:

$R_M = 1 + Na^M + Na^M Cl^M + Na^M Cl^M K^M + Na^M Cl^M K^M Cl''^M$

$R_N = 1 + Cl''^N + K^N Cl''^N + Cl^N K^N Cl''^N + Na^N Cl^N K^N Cl''^N$

$R_{MM} = g^M_E + g^M_{ENaClKCl} Na^M Cl^M K^M Cl''^M$

$R_{NN} = g^N_E + g^N_{ENaClKCl} Na^N Cl^N K^N Cl''^N$

Weinstein et al., in 2009 [141], considered the order of binding for NKCC as Benjamin's group (i.e., Na^+, Cl, K, and the second Cl and for the dissociation to happen as Na^+ first, Cl^-, K^+, and the second Cl^-). However, in their model, they considered competition between ammonium and potassium ions for the same binding site [141]. Here, their model is transformed to the general form of the resistance parameters from and net uptake flux of Na^+ and K^+ are expressed in eqs. (126a) and (126b), respectively.

$$\boxed{J^{M,N(net)}_{Na,NKCC} = [E]_t \left(\frac{g^N_E R_{MM} - g^M_E R_{NN}}{R_M R_{NN} + R_N R_{MM}} \right)} \tag{126a}$$

$$\boxed{J^{M,N(net)}_{K,NKCC} = [E]_t \left(\frac{\left(g^M_{ENKCC} Na^M K^M (Cl^M)^2\right) R_{NN} - \left(g^N_{ENKCC} Na^N K^N (Cl^N)^2\right) R_{MM}}{R_M R_{NN} + R_N R_{MM}} \right)} \tag{126b}$$

where $[E]_t = R_M [E]_M + R_N [E]_N$ represents the total carrier concentration of the KCC transporter on either side of the membrane. $[E]$ represents the concentration of the empty NKCC carrier. R_M, R_N, R_{MM}, and R_{NN} are the resistance parameters and defined as:

$R_M = 1 + Na^M + Na^M Cl^M + Na^M K^M Cl^M + Na^M K^M (Cl^M)^2 + Na^M {NH_4}^M Cl^M + Na^M NH^M_4 (Cl^M)^2$

$R_N = 1 + Cl^N + K^N Cl^N + K^N (Cl^N)^2 + Na^N K^N (Cl^N)^2 + NH^N_4 Cl^N + {NH_4}^N (Cl^N)^2 + Na^N NH^N_4 + (Cl^N)^2$

$R_{MM} = g^M_E + g^M_{ENKCC} Na^M K^M (Cl^M)^2 + g^M_{ENNH_4CC} Na^M {NH_4}^M (Cl^M)^2$

$R_{NN} = g^N_E + g^N_{ENKCC} Na^N K^N (Cl^N)^2 + g^N_{ENNH_4CC} Na^N {NH_4}^N (Cl^N)^2$

K_{ion} is the equilibrium constant of the ion in the unit of *mmol*. By applying the symmetry assumption for the equilibrium constant coefficients on the two sides of the membrane, there is no "M" or "N", designation and the normalized concentrations can be expressed as

$Na^M = \frac{[Na]_M}{K_{Na}}$, $K^M = \frac{[K]_M}{K_K}$, $Cl^M = \frac{[Cl]_M}{K_{Cl}}$, ${NH_4}^M = \frac{[NH_4]_M}{K_{NH_4}}$

$Na^N = \frac{[Na]_N}{K_{Na}}$, $K^N = \frac{[K]_N}{K_K}$, $Cl^N = \frac{[Cl]_N}{K_{Cl}}$, $NH_4{}^N = \frac{[NH_4]_N}{K_{NH_4}}$

NKCC transporters can also be modeled by using the simple model. Here, two simplified models are presented: eq. (127) and eq. (131).

A commonly used reduced NKCC model initially developed by Verkman and Alpern in 1987 [142] and later was reparametrized in Figure 17 of [20]. In this simplified model, the rapid equilibrium assumption, quasi-steady-state assumption, and symmetric carrier assumption are discussed. Furthermore, it is assumed that the binding and unbinding steps do not follow a particular sequential order. Under these assumptions, the net outward NKCC turnover rate is given by eq. (127), and the transported flux of Na, Cl, and K ions can be obtained from eqs. (128), (130), and (129), respectively [38].

$$\boxed{J^{M-N}_{NKCC2} = P^{symporter}_{NKCC2} \frac{[Na]_{M(e)}[K]_{M(e)}[Cl]^2_{M(e)} - [Na]_{N(i)}[K]_{N(i)}[Cl]^2_{N(i)}}{\left[\frac{[Na]_{N(i)}}{K_{Na}} + 1\right]\left[\frac{[K]_{N(i)}}{K_K} + 1\right]\left[\frac{[Cl]_{N(i)}}{K_{Cl}} + 1\right]^2}} \tag{127}$$

$$\boxed{J^{M,N(net)}_{Na,NKCC2} = J^{M,N(net)}_{NKCC2}} \tag{128}$$

$$\boxed{J^{M,N(net)}_{K,NKCC2} = J^{M,N(net)}_{NKCC2}} \tag{129}$$

$$\boxed{J^{M,N(net)}_{Cl,NKCC2} = 2J^{M,N}_{NKCC2}} \tag{130}$$

Here, J_{NKCC2} is the turn over rate of transporter NKCC, in the units of $\mu eq.cm^{-2}.h^{-1}$ (defined as positive for the flux into the cell) and P_{NKCC2} is the permeability coefficient for the transporter NKCC2.

Eq. (131) represents one other simplified model developed by Palk et al. [37] to obtain the net outward NKCC turnover rate.

$$\boxed{J_{NKCC} = [E]_{NKCC}\left(r_{NKCC}\frac{1 - \alpha_1[Na]_i[K]_i[Cl]^2_i}{K_{NKCC} + \alpha_2[Na]_i[K]_i[Cl]_i{}^2}\right)} \tag{131}$$

where $[E]t$ is the NKCC transporter density per membrane area, r_{NKCC} is a constant in the unit of $1/s$, α_1 and α_2 are dimensionless constants, K_{NKCC} is a constant in a unit of mM^{-4} [37, 143].

5.2. *Potassium Chloride Symporter (KCC)*

The potassium chloride symporter is a membrane transporter that functions in the electroneutral movement of potassium (K^+) and Cl^- across the plasma membrane of many cells [144], including the renal proximal tubule [145] and the neuron [146]. It contributes to renal chloride reabsorption and to transport chloride across the basolateral membrane with a stoichiometric ratio of $1K^+ : 1Cl^-$. This suggests that the transmembrane voltage does not drive the overall transport process of K^+ and Cl^- via the KCC, and the transport process does not directly generate a membrane current that may change the transmembrane voltage [147, 148]. Moreover, the KCC cotransporter is bidirectional and can mediate net ion efflux or influx. Depending on the dominant K^+ and Cl^- chemical potential gradients and the physiological ranges of intracellular Cl^- and extracellular K^+ concentrations, KCCs can act to either extrude or store chloride ions [144, 149]. KCC cotransporters may also transport ammonium, which competes with potassium (K) for the same binding sites on the carrier [150, 151].

Figure 16 of [20] represents a competitive KCC transport mechanism of potassium, chloride, and ammonium ions, in which ammonium competes with potassium for the same binding sites on the KCC. In this configuration, in the first step, Cl ion (A in Figure 16 of [20]) binds to the empty carrier (E), followed by the binding of K ions (B in Figure 16 of [20]) or NH_4 (C in Figure 16 of [20]) ions to form the complex $EClK$ or $EClNH_4$, respectively. Next, the formed complexes cross the membrane ($EClK_N$ or $EClNH4_N$), where they undergo dissociation reactions in which Cl unbinds last from both complexes. In this model, it is assumed that the carrier can exist in four different states on each side of the membrane and that only the fully loaded (EClK and EClNH4) and empty carriers (E) can cross the membrane. Under equilibrium and steady-state assumptions, net outward fluxes of Cl, K and NH4 can be obtained through eqs. (132c), (132a), and (132b), respectively.

$$\boxed{J^{M,N(net)}_{K,KCl} = [E]_t \frac{\left(g^M_{EClK} Cl^M K^M\right) R_{NN} - \left(g^N_{EClK} Cl^N K^N\right) R_{MM}}{R_M R_{NN} + R_N R_{MM}}} \tag{132a}$$

$$\boxed{J^{M,N(net)}_{NH_4,KCl} = [E]_t \frac{\left(g^M_{EClNH_4} Cl^M NH_4^M\right) R_{NN} - \left(g^N_{EClNH_4} Cl^N NH_4^N\right) R_{MM}}{R_M R_{NN} + R_N R_{MM}}} \tag{132b}$$

$$J^{M,N(net)}_{Cl,KCl} = [E]_t \frac{\left(g^M_{EClK} Cl^M \beta^M + g^M_{EClNH_4} Cl^M NH^M_4\right) R_{NN} - \left(g^N_{EClK} Cl^N K^N + g^N_{EClNH_4} Cl^N NH^N_4\right) R_{MM}}{R_M R_{NN} + R_N R_{MM}} \tag{132c}$$

where $[E]_t = [E]_M + [ECl]_M + [EClK]_M + [EClNH_4]_M + [EClNH_4]_N + [EClK]_N + [ECl]_N + [E]_N$. K_{ion} is the equilibrium constant of the ion in the unit of *mmol* and the normalized concentrations are: $Cl^M = \frac{[Cl]_M}{K^M_{Cl}}$, $K^M = \frac{[K]_M}{K^M_K}$, $NH^M_4 = \frac{[NH4]_M}{K^M_C}$ | $Cl^N = \frac{[A]_N}{K^N_{Cl}}$, $K^N = \frac{[K]_N}{K^N_B}$, $NH^N_4 = \frac{[NH_4]_N}{K^N_{NH_4}}$

The resistance parameters are defined as:

$R_M = 1 + Cl^M + Cl^M K^M + Cl^M NH^M_4$ | $R_N = 1 + Cl^N + Cl^N K^N + Cl^N NH^N_4$

$R_{MM} = g^M_E + g^M_{EClK} Cl^M K^M + g^M_{EClNH_4} Cl^M NH^M_4$ | $R_{NN} = g^N_E + g^N_{EClK} Cl^N K^N + g^N_{EClNH_4} Cl^N NH^N_4$

In the absence of the NH^+_4 competitor (i.e., $J_{NH4^+,KCl} = 0$) the values for NH_4 related terms become zero (i.e., $\gamma^N = \gamma^M = 0$, $NH^M_4 = NH^N_4 = 0$, and $g^M_{EClNH_4} = g^N_{ECLNH_4} = 0$), and the net flux of the Cl^- is expressed by eq. (133) while the K flux still can be obtained through eq. (132a).

$$J^{KCl}_{Cl^-} = [E]_t \frac{\left(g^M_{EClK} Cl^M \beta^M\right) R_{NN} - \left(g^N_{EClK} Cl^N K^N\right) R_{MM}}{R_M R_{NN} + R_N R_{MM}} \tag{133}$$

In 2010, Weinstein [112] developed a model for KCC to compute the unidirectional fluxes through chloride potassium with ammonium transport by assuming rapid equilibrium. Weinstein [112] considered the first-on first-off binding mechanism for the KCC symporter, where potassium (K) ions or ammonium ions (NH_4) are the first ions that bind to the transporter, and they unbind first. In the first step, either potassium ion (K^+) or ammonium (NH_4) ion (which competes with potassium ion for the same binding site) binds to the empty carrier (E) and forms the complexes EK or $ENH4$, respectively. This step is followed by the binding of chloride ions and the formation of $EKCl$ and $ENH4Cl$ complexes. Next, the formed complexes cross the membrane ($EKCl_N$ or $ENH4Cl_N$), where they undergo dissociation reactions in which Cl unbinds last from both complexes. In this model, it is assumed that only the fully loaded (EKCl and ENH4Cl) and empty carriers (E) can cross the membrane [112]. Under equilibrium and steady-state assumptions, net outward fluxes of K, NH4, and Cl can be obtained through eqs. (134a), (134b), and (134c) respectively [112].

$$\boxed{J^{M,N(net)}_{K,KCC} = [E]_t \left(\frac{\left(g^M_{EKCl} K^M Cl^M\right) R_{NN} - \left(g^N_{EKCl} K^N Cl^N\right) R_{MM}}{R_M R_{NN} + R_N R_{MM}} \right)} \tag{134a}$$

$$\boxed{J^{M,N(net)}_{NH_4,KCl} = [E]_t \frac{\left(g^M_{ENH_4Cl} NH^M_4 Cl^M\right) R_{NN} - \left(g^N_{ENH_4Cl} NH^N_4 Cl^N\right) R_{MM}}{R_M R_{NN} + R_N R_{MM}}} \tag{134b}$$

$$\boxed{J^{M,N(net)}_{Cl,KCl} = [E]_t \frac{\left(g^M_{EKCl} K^M Cl^M + g^M_{ENH_4Cl} NH^M_4 Cl^M\right) R_{NN} - \left(g^N_{EKCl} K^N Cl^N + g^N_{ENH_4Cl} NH^N_4 Cl^N\right) R_{MM}}{R_M R_{NN} + R_N R_{MM}}} \tag{134c}$$

where $[E]_t = R_M[E]_M + R_N[E]_N$ represents the total carrier concentration of the KCC transporter on either side of the membrane. $[E]$ is the concentration of the empty carrier. R_M, R_N, R_{MM}, and R_{NN} are the resistance parameters and defined as:

$R_M = 1 + K^M + K^M Cl^M + NH^M_4 Cl^M \mid R_N = 1 + Cl^N + K^N Cl^N + NH^N_4 Cl^N$

$R_{MM} = g^M_E + g^M_{EKCl} K^M Cl^M + g^M_{ENH_4Cl} NH^M_4 Cl^M \mid R_{NN} = g^N_E + g^N_{EKCl} K^N Cl^N + g^N_{ENH_4Cl} NH^N_4 Cl^N$

K_{ion} is the equilibrium constant of the ion in the unit of *mmol* and the normalized concentrations are: $K^M = \frac{[K]_M}{K^M_K}$, $Cl^M = \frac{[Cl]_M}{K^M_{Cl}}$, $NH^M_4 = \frac{[NH4]_M}{K^M_C} \mid K^N = \frac{[K]_N}{K^N_B}$, $Cl^N = \frac{[A]_N}{K^N_{Cl}}$, $NH^N_4 = \frac{[NH_4]_N}{K^N_{NH_4}}$

5.3. Sodium chloride cotransporter (NCC)

The sodium chloride cotransporter (NCC) is a member of the family of electroneutral cation-coupled chloride cotransporters that is exclusively expressed in the apical membrane of the distal convoluted tubule segment of the kidney nephron [152]. NCC is vital for maintaining fluid and salt balance, as it functions in reabsorbing sodium and chloride ions from the tubular fluid into the cells of the distal convoluted tubule of the nephron [153].

Weinstein in 2005 [154] developed a model to obtain the ion flux transported by NCC based on the kinetic characterization of NCC. This model is also depicted in Figure 11 of [20], where A and B refer to Na and Cl ions, respectively, and only the fully loaded carrier can cross the membrane, and the partially loaded carriers cannot translocate across the membrane (i.e., $g_{EA} = g_{EB} = 0$) [20, 154]. In the NCC model (developed by Weinstein [154]), the NCC carrier can be oriented toward the M surface of the membrane, where either Na or Cl may bind to it to form the complex ENa_M or ECl_M, respectively. Next, these complexes undergo another association reaction to form

the fully loaded carrier-solute complex ($ENaCl_M$).

In this configuration, it is assumed that there are no restrictions on the order of binding, and only the empty carrier and fully loaded carrier can cross the membrane, and the partially loaded carriers cannot translocate across the membrane (i.e., $g_{EA} = g_{EB} = 0$). Under equilibrium and steady-state assumptions, net outward transported fluxes of sodium (Na) and chloride (Cl) ions by NaCl cotransporter can be obtained through eqs. (135a) and (135b), respectively [20, 154].

$$\boxed{J^{M,N(net)}_{Na,NCC} = [E]_t \left(\frac{(g^M_{ENaCl} Na'^M Cl^M)(g^N_E) - (g^N_{ENaCl} Na'^N Cl^N)(g^M_E)}{R_M R_{NN} + R_N R_{MM}} \right)} \tag{135a}$$

$$\boxed{J^{M,N(net)}_{Cl,NCC} = [E]_t \left(\frac{(g^M_{ENaCl} Na'^M Cl^M)(g^N_E) - (g^N_{ENaCl} Na'^N Cl^N)(g^M_E)}{R_M R_{NN} + R_N R_{MM}} \right)} \tag{135b}$$

where $[E]_t = [E]_M + [ECl]_M + [ENa]_M + [ENaCl]_M + [ENaCl]_N + [ENa]_N + [ECl]_N + [E]_N$ represents the total carrier concentration of the NCC transporter on either side of the membrane. R_M, R_N, R_{MM}, and R_{NN} are the resistance parameters and defined as:

$R_M = (1 + Na^M + Cl^M + Na'^M Cl^M) \mid R_N = (1 + Na^N + Cl^N + Na'^N Cl^N)$

$R_{MM} = g^M_E + g^M_{ENaCl} Na'^M Cl^M \mid R_{NN} = g^N_E + g^N_{ENaCl} Na'^N Cl^N$

K_{ion} is the equilibrium constant of the ion in the unit of *mmol* and the normalized concentrations are: $Na^M = \frac{[Na]_M}{K^M_{Na}}$ $Na'^M = \frac{[Na]_M}{K^M_{ClNa}}$ $Cl^M = \frac{[Cl]_M}{K^M_{Cl}} \mid Na^N = \frac{[Na]_N}{K^N_{Na}}$ $Na'^N = \frac{[Na]_N}{K^N_{ClNa}}$ $Cl^N = \frac{[Cl]_N}{K^N_{Cl}}$

5.4. Sodium Bicarbonate Cotransporter (NBC)

The sodium bicarbonate cotransporter (NBC) plays an essential role in the acid-base balance of the cell and in regulating intracellular pH in a variety of cells [155, 156] such as neurons [156–158], cardiac myocytes [159–161], vascular smooth muscle [156, 162, 163], and fibroblasts [155, 164, 165]. The transport direction through NBCs can be inward or outward, and they can be categorized as electrogenic (NBCe) or neutral (NBCn) [166]. Electrogenic NBCs (NBCs) play key roles in bicarbonate anion (HCO_3^-) reabsorption by the renal proximal tubule and HCO_3^- secretion by the pancreatic duct ($1HCO_3 : 1Na$ stoichiometry). Electroneutral NBC (NBCn) regulates pH in vascular smooth muscle and is expressed in/near axons in the brain [156].

Over the years, for both electroneutral and electrogenic families of the NBCs (i.e., *NBCn*

and $NBCe$), several models have been developed that can be used to mathematically describe the turnover rate of the NBC transporter. Some of the well-known models are discussed below.

Sohma et al. in 2000 [167], considered a general $1Na : nHCO_3$ electrogenic cotransporter, $NBCe$, and developed a model for the $NBCe$ turnover rate. They used a six-state kinetics scheme [168] to quantitatively describe the kinetics of NBCe in renal proximal tubule cells. This kinetic scheme is also depicted in Figure 12 of [20], where A and B refer to Na and $nHCO_3$ ions, respectively. Sohma et al. [167] assumed the following: (1) HCO_3 ions are lumped together, and the symporter has a single binding site that binds Na ions and HCO_3 ions with sequential binding steps; only the empty carrier and the fully loaded carrier can cross the membrane (i.e., the partially loaded carriers cannot translocate across the membrane). (2) that dissociation constants for each ion at intracellular and extracellular sides of the membrane are the same (i.e., $K_{Na}^{M-N} = K_{Na}^{N-M} = K_{Na}$ and $K_{HCO_3}^{M-N} = K_{HCO_3}^{N-M} = K_{HCO_3}$) (3) the kinetic at $V_m^{M-n(bl)} = 0$ the translocation velocity for the fully loaded carrier and empty carrier from outside to inside and inside to outside were the same (i.e., $g_{ENanHCO_3}^{M-N} = g_{ENanHCO_3}^{N-M} = g_{ENanHCO_3}$ and $g_E^{M-N} = g_E^{N-M} = g_E$) (4) finally, the translocation step between of the loaded carrier from inside to outside or outside to inside is voltage-dependent (that is, the kinetic steps between the intracellular loaded carrier ($ENanHCO_{3M(i)}$) and the extracellular loaded carrier ($ENanHCO_{3N(o)}$) is voltage independent) but the translocation step between E_i (intracellular empty carrier) and E_o (extracellular empty carrier) is voltage-dependent (carrying the net charge of $n-1$) [168]. Under these assumptions, the turnover rate of the electrogenic [167]. Under these assumptions, the turnover rate of the electrogenic $Na^+ - nHCO_3^-$ cotransporter, $NBCe$, can be obtained by eq. (136a).

$$J_{NBCe} = P_{NBCe} \times \frac{\left(\frac{[Na]_{bl}[HCO3]_{bl}^n}{K_{Na}K_{HCO3}^n}\right)\times\phi_1 - \left(\frac{[Na]_c[HCO3]_c^n}{K_{Na}K_{HCO3}^n}\right)\times\phi_2}{\left(\phi_2 + g'\left(\frac{[Na]_{bl}[HCO3]_{bl}^n}{K_{Na}K_{HCO3}^n}\right)\right)\left(1 + \frac{[Na]_c}{K_{Na}} + \frac{[Na]_c[HCO3]_c^n}{K_{Na}K_{HCO3}^n}\right) - \left(\phi_1 + g'\left(\frac{[Na]_c[HCO3]_c^n}{K_{Na}K_{HCO3}^n}\right)\right)\left(1 + \frac{[Na]_c}{K_{Na}} + \frac{[Na]_{bl}[HCO3]_{bl}^n}{K_{Na}K_{HCO3}^n}\right)} \tag{136a}$$

$$\phi_1 = exp\left(\frac{-(1-n)FV_m^{M-N(bl)}}{2RT}\right) \tag{136b}$$

$$\phi_2 = exp\left(\frac{(1-n)FV_m^{M-N(bl)}}{2RT}\right) \tag{136c}$$

where ϕ_1 and ϕ_2 define the dependency of the $NBCe$ translocation rate on membrane voltage and can be obtained through eqs. (136b) and (136c). P_{NBCe} is the membrane permeability to the $NBCe$ symporter, $'n'$ is the coupling ratio of HCO_3 ions to one Na ion in the NCB_e cotransporter, g' is the velocity constant ratio of the translocation step of the fully loaded carrier to the empty carrier (i.e., $g' = \frac{g_{ENanHCO_3}}{g_E}$), and K_{Na} and K_{HCO_3} are the dissociation constant for binding of Na and HCO_3 ions to $NBCe$, respectively.

In 2004, Whitcomb et al. [103] used the proximal rat duct cell model [167] and developed a simplified model for the $1Na : nHCO_3$ electromagnetic cotransporter ($NBCe$) model for the proximal pancreatic duct cell. They reduced Sohma et al.'s complex model [167] to one simplified linear model that can be used to compute the turnover rate of the $NBCe$ cotransporter. Their model is given in eq. (137).

$$\boxed{J_{NBCe} = g_{nbc}(V_m - E_{nbc})} \tag{137}$$

where

$$E_{nbc} = \frac{RT}{F(n-1)} ln \frac{[Na]_i [HCO3]_i^n}{[Na]_o [HCO3]_o^n} \tag{138}$$

The $1Na : 1HCO_3$ electroneutral cotransporter, NBCn, can follow the six-state kinetic mechanism depicted in Figure 12 of [20], where A and B refer to Na^+ and HCO_3^-, respectively, and M and N refer to the two sides of the cell membrane. In this configuration, in the first step, the carrier faces the intracellular side (M side) of the membrane and binds to Na^+ ions. After the complex ENa_M is formed, a HCO_3 ion binds to ENa_M to form the $ENaHCO_{3M}$ complex to give the fully loaded carrier complex ENaHCO3M. In this model, similar to Sohma's model ([167]), only the empty carrier (E) and the fully loaded carrier ($ENaHCO_3$) can translocate across the membrane, and the unbinding reactions occur in the reverse order of binding (i.e., on the other side of the membrane, the first HCO_3 ion unbinds from the translocated loaded carrier, and then the Na+ ion unbinds). Under these assumptions, the steady-state turnover rate of the NBCn can be obtained through eq. (139a) and corresponding fluxes for sodium and bicarbonate ions can be obtained through eqs.

(139b) and (139c), respectively [20, 168].

$$\boxed{J_{NBCn}^{M,N(net)} = [E]_t \frac{(g_{ENaHCO_3}^{M} Na^M HCO_3^M) g_E^N - (g_{ENaHCO_3}^{N} Na^N HCO_3^N) g_E^M}{R_M R_{NN} + R_N R_{MM}}} \tag{139a}$$

$$\boxed{J_{Na,NBCn}^{M,N(net)} = J_{NBC}^{M,N(net)}} \tag{139b}$$

$$\boxed{J_{HCO_3,NBCn}^{M,N(net)} = J_{NBC}^{M,N(net)}} \tag{139c}$$

where $[E]_t = [E]_M + [ENa]_M + [ENaHCO_3]_M + [ENaHCO_3]_N + [ENa]_N + [E]_N$ represents the total carrier concentration of the NBCn transporter on either side of the membrane. R_M, R_N, R_{MM}, and R_{NN} are the resistance parameters and defined as:

$R_M = (1 + Na^M + Na^M HCO_3^M) \mid R_N = (1 + Na^N + Na^N HCO_3^N)$

$R_{MM} = (g_E^M + g_{ENaHCO_3}^{M} Na^M HCO_3^M) \mid R_{NN} = (g_E^N + g_{ENaHCO_3}^{N} Na^N HCO_3^N)$

K_{ion} is the equilibrium constant of the ion in the unit of *mmol* and the normalized concentrations are: $Na^M = \frac{[A]_M}{K_{Na}^M}$, $HCO_3^M = \frac{[HCO_3]_M}{K_{NaHCO_3}^M} \mid Na^N = \frac{[Na]_N}{K_{Na}^N}$, $HCO_3^N = \frac{[HCO_3]_N}{K_{NaHCO_3}^N}$

Fong et al. [36] developed a simplified model for the electroneutral sodium bicarbonate co-transporter that transports both Na and HCO_3 in the same direction. Their model is given in eq. (140) [36].

$$\boxed{J_{NBCn} = n_{NBCn}^{''} \frac{k_5^+ k_6^+ [Na^+]_{cell(i)} [HCO3^-]_{cell(i)} - k_5^- k_6^- [Na^+]_e [HCO3^-]_e}{k_5^+ [Na^+]_i [HCO3^-]_i + k_5^- k_6^+ + k_6^- [Na^+]_e [HCO3^-]_e}} \tag{140}$$

where $n_{NBCn}^{''}$ is $NBCn$ density per membrane area, k_5^+, k_5^-, k_6^+, k_6^- are rate constant in $mM.s^{-1}$.

5.5. Sodium Phosphate cotransporter (NPT)

The sodium-phosphate cotransporter (NPT), also known as the sodium-dependent phosphate transporter, plays a central role in phosphate transport and maintains normal cellular functions such as cellular metabolism, signal transduction, nucleic acid synthesis, and lipid synthesis [169]. NPTs use the sodium-electrochemical gradient to drive phosphate translocation against its concentration gradient and absorb phosphate ions from the interstitial fluid. The sodium-phosphate cotransporter family members differ in their Na:Pi stoichiometry, and they are categorized as elec-

trogenic and electroneutral. The electrogenic NPTs transport three sodium ions per phosphate molecule ($3Na^+ : Pi$ cotransport stoichiometries), while the electroneutral NPT transports two sodium ions per phosphate ($2Na^+ : Pi$ cotransport stoichiometries) [170, 171].

Elmariah et al. proposed a kinetic model for sodium-phosphate cotransporter that displays $2Na : 1HPO_4$ stoichiometry (electroneutral NPT) [172]. Their kinetic scheme is identical to the kinetic scheme shown in Figure 14 of [20]. In this kinetic scheme, the NPT carrier, E, transports sodium ions (Na) and phosphate ions (PO_4) in a ratio of $2Na : PO_4$ in a sequential binding order manner. In the first step, the carrier faces the M side of the membrane and binds to a Na ion. After the complex ENa_M is formed, an ion of HPO_4 binds to ENa_M to form the $ENaPO_{4M}$ complex, followed by the binding of a second ion of Na^+ to form the fully loaded carrier $ENaHPO_4Na_M$. In this model, the carriers can translocate across the membrane in all states (i.e., in the empty, partially loaded, and fully loaded states), and the unbinding reactions occur in the reverse order of binding. The net outward fluxes of sodium ions (Na^+) and phosphate ions (PO_4) transported via the cotransporter are obtained by eqs. (141a) and (141b), respectively [20, 172].

$$J^{M,N(net)}_{Na,NaPO_4} = [E]_t\left(\frac{R_{NN}\left(g^M_{ENa}Na^M + g^M_{ENaPO_4}Na^MPO^M_4 + g^M_{ENaPO_4Na}Na^MPO^M_4Na''^M\right)}{R_MR_{NN} + R_NR_{MM}} - \frac{R_{MM}\left(g^N_{EA}Na^N + g^N_{ENaPO_4}Na^NPO^N_4 + g^N_{ENaPO_4Na}Na^NPO^N_4Na''^N\right)}{R_MR_{NN} + R_NR_{MM}}\right) \tag{141a}$$

$$J^{M,N(net)}_{PO_4,NaPO_4} = [E]_t\left(\frac{R_{NN}\left(g^M_{ENaPO_4}Na^MPO^M_4 + g^M_{ENaPO_4Na}Na^MPO^M_4Na''^M\right)}{R_MR_{NN} + R_NR_{MM}} - \frac{R_{MM}\left(g^N_{ENaPO_4}Na^NPO^N_4 + g^N_{ENaPO_4Na}Na^NPO^N_4Na''^N\right)}{R_MR_{NN} + R_NR_{MM}}\right) \tag{141b}$$

where $[E]_t = [E]_M + [ENa]_M + [ENaPO_4]_M + [ENaPO_4Na]_M + [ENaPO_4Na]_N + [ENaPO_4]_N + [ENa]_N + [E]_N$ represents the total carrier concentration of the NBCn transporter on either side of the membrane. R_M, R_N, R_{MM}, and R_{NN} are the resistance parameters and defined as:

$R_M = 1 + Na^M + Na^MPO^M_4 + Na^MPO^M_4Na''^M \mid R_N = 1 + Na^N + Na^NPO^N_4 + Na^NPO^N_4Na''^N$

$R_{MM} = g^M_E + g^M_{ENa}Na^M + g^M_{ENaPO_4}Na^MPO^M_4 + g^M_{ENaPO_4Na}Na^MPO^M_4Na''^M$

$R_{NN} = g^N_E + g^N_{ENa} Na^N + g^N_{ENaPO_4} Na^N PO^N_4 + g^N_{ENaPO_4Na} Na^N PO^N_4 Na''^N$

K_{ion} is the equilibrium constant of the ion in the unit of *mmol* and the normalized concentrations are:

$Na^M = \frac{[Na]_M}{K^M_{Na}}$, $PO^M_4 = \frac{[PO_4]_M}{K^M_{NaPO_4}}$, $Na''^M = \frac{[Na]_M}{K^M_{NaPO_4Na}}$ | $Na^N = \frac{[Na]_N}{K^N_{Na}}$, $PO^N_4 = \frac{[PO_4]_N}{K^N_{NaPO_4}}$, $Na''^N = \frac{[Na]_N}{K^N_{NaPO_4Na}}$

5.6. Sodium Glucose Symporter (SGLT)

The sodium-glucose transporter (SGLT) is a carrier that uses the electrochemical potential gradient produced during the transport of sodium ions to import glucose molecules into the cell in the opposite direction of its gradients. During this transport, glucose and sodium ions move in the same direction, while glucose utilizes the energy produced from transporting the sodium ions with $1Na^+ : 1glucose$ stiochiometry [173]. The electrogenic Na-coupled glucose transporter follows a six-state kinetic mechanism (similar to Figure 13 of [20]), where some of the rate constants may be dependent on the membrane potential [174–176]. However, the effect of membrane potential on the resistance parameters (R terms) in the flux equation must be considered individually by checking their definitions individually and checking whether they have rate-limiting translocation rate constants (e.g, g_E or g_{EA}). More details about the kinetic properties of the electrogenic Na-coupled glucose transporter, such as the identification of rate-limiting steps and of the voltage dependence (translocation and/or Na binding), can be found in [106, 177].

Here, we represent a simplified model to calculate the net glucose transported flux by electrogenic Na-coupled transporters developed by Verkman et al. [142]. Their model is expressed in eq. (142) [142].

$$J^{M-N(a)}_{SGLT} = P^{M-N(a)}_{SGLT} exp\left(\frac{V^{M-N(a)}_m F}{RT}\right) \frac{[glucose]_N[Na]_N - [glucose]_M[Na]_M exp\left(-\frac{V^{M-N(a)}_m F}{RT}\right)}{1 - exp\left(-\frac{V^{M-N(a)}_m F}{RT}\right)} \quad (142)$$

where $P^{M-N(a)}_{SGLT}$ is the permeability of the membrane to SGLT per $1cm^2$ of the membrane $(mol/s/cm^2)$, V^{M-N}_m is the membrane voltage, F is the Faraday's constant, R is the universal gas constant, and T is the temperature in Kelvin.

5.7. Amino Acid Transporters (AAT)

Amino acid molecules can be transported across the cell membrane using the energy produced during the sodium ion transport process. The sodium-amino acid transport mechanism can be modeled similarly to the sodium-glucose transport mechanism. Therefore, the sodium flux transported by amino acid transporters can be obtained by using eq. (143), which was developed by Verkman et al. (1987) [142].

$$J_{AAT}^{M-N(a)} = P_{AAT}^{M-N(a)} exp\left(\frac{V_m^{M-N(a)} F}{RT}\right) \times \frac{[AminoAcid]_N [Na]_N - [AminoAcid]_M [Na]_M exp\left(-\frac{V_m^{M-N(a)} F}{RT}\right)}{1 - exp\left(-\frac{V_m^{M-N(a)} F}{RT}\right)}$$

where $J_{AAT}^{M-N(a)}$ is the turn over rate of the Na-coupled amino acid cotransporter, $P_{AAT}^{M-N(a)}$ is the permeability of the membrane to the Na-coupled amino acid transporter per $1cm^2$ of the membrane $(mol/s/cm^2)$, V_m^{M-N} is the membrane voltage, F is the Faraday's constant, R is the universal gas constant, and T is the temperature in Kelvin.

6. Excheangers

This section includes several kinetic models of exchangers (antiporters), namely, bicarbonate chloride exchanger (BCE) (section 6.1), sodium calcium exchanger (section 6.2), and sodium hydrogen exchanger (NHE) (section 6.3).

6.1. Bicarbonate Chloride exchanger (BCE)

Bicarbonate chloride exchanger (BCE) is an electroneutral antiporter that allows the exchange of bicarbonate ions for chloride ions across the cellular membrane and plays an essential role in both secretory and nonsecretory cells. The existence of the bicarbonate chloride anion exchanger on the apical membrane of secretory and epithelial cells has been reported in several studies [178, 179]. The presence of this exchanger on the apical face results in fluid and HCO3 secretion into the lumen. More information about the physiology of this anion exchanger can be found in [21, 36].

675 The transport direction of HCO_3 ions is from (internal) M to (external) N, and Cl ion movement
676 occurs simultaneously in the opposite direction.

Weinstein in 2000 [180] developed a model to obtain the ion flux transported by BCEs. This model is also depicted in Figure 20 of [20]. In this depicted mechanism, termed the "ping-pong" mechanism, the anion exchanger, BCE, has a single binding site (transport site) to which Cl ions and HCO_3 ions competitively bind, and only loaded and empty carriers can cross the membrane. In the first step, HCO_3 ions bind to the membrane carrier on the outside surface. Assuming that the binding of chloride to the carrier occurs simultaneously on the other side of the membrane, HCO_3-carrier ($EHCO_3$) and Cl-carrier (ECl) complexes are formed on opposite sides of the membrane. After translocation of the formed complexes, each of the complexes undergoes a dissociation reaction. These dissociation reactions lead to the release of HCO_3 ions and Cl ions from the N (inside) and M (outside) faces of the membrane, respectively. Under the rapid binding assumption, the chloride and bicarbonate ion fluxes through the chloride bicarbonate exchanger (BCE) can be obtained through eqs. (143a) and (143b), respectively.

$$\boxed{J_{Cl,BCE} = E_t \frac{[g^M_{EHCO_3} g^N_{ECl} HCO^M_3(Cl^N) - g^N_{EHCO_3} g^M_{ECl} HCO^N_3(Cl^M)]}{R_M R_{00} + R_N R_{ee}}} \tag{143a}$$

$$\boxed{J_{HCO3,BCE} = E_t \frac{[g^M_{EHCO_3} g^N_{ECl} (Cl^M HCO^N_3) - g^N_{EHCO_3} g^M_{ECl} (Cl^N HCO^M_3)}{R_M R_{00} + R_N R_{ee}}} \tag{143b}$$

677 where $[E]_t = [E]_M + [EHCO_3]_M + [ECl]_M + [E]_N + [EHCO_3]_N + [ECl]_N$

678 $HCO^M_3 = \frac{[HCO_3]_M}{K^M_{HCO_3}}, Cl^M = \frac{[Cl]_M}{K^M_{Cl}} \mid HCO^N_3 = \frac{[HCO_3]_N}{K^N_{HCO_3}}, Cl^N = \frac{[Cl]_N}{K^N_{Cl}}$

679 $R_M = 1 + HCO^M_3 + Cl^M \mid R_N = 1 + HCO^N_3 + Cl^N$

680 $R_{MM} = g^M_{EHCO_3} HCO^M_3 + g^M_{ECl}\, Cl^M \mid R_{NN} = g^N_{EHCO_3} HCO^N_3 + g^N_{ECl}\, Cl^N$

Sohma et al. in 1996 [22] developed a simplified model for BCE, which is represented in Figure 22 of [20]. In using this model, A and B refer to Cl ions and HCO_3 ions, respectively, and for a BCE located on the apical membrane, M refers to the luminal region and i refers to the intracellular region (i.e., $M = l$, and $N = i$). The turn over rate of the BCE transporter can be

obtained through eq. (144)

$$J_{BCE} = P_{BCE} \frac{[Cl]_l[HCO3]_c - [Cl]_c[HCO3]_l}{K_{Cl}K_{HCO3}\Big((1 + \frac{[Cl]_c}{K_{Cl}} + \frac{[HCO3]_c}{K_{HCO3}})(\frac{[Cl]_l}{K_{Cl}} + \frac{[HCO3]_l}{K_{HCO3}}) + (1 + \frac{[Cl]_l}{K_{Cl}} + \frac{[HCO3]_l}{K_{HCO3}})(\frac{[Cl]_c}{K_{Cl}} + \frac{[HCO3]_c}{K_{HCO3}})\Big)} \tag{144}$$

where J_{BCE} is the turn over rate of the Cl/HCO_3 exchanger ($nmol/min/cm^2$), $P_{BCE} = g_{BCE}[E_t]$ is the permeability of the membrane to BCE per $1cm^2$ of the membrane ($mol/s/cm^2$), and K_{Cl} and K_{HCO_3} are the dissociation constants for Cl and HCO_3, respectively in the unit of mM.

Fong et al. [21, 36] developed a more simplified model for calculating the BCE turnover rate. For simplicity, they assumed that the transport kinetics for all states of the carrier (all isoforms) and ligand binding steps are identical and defined the positive direction of flux as chloride ions entering the cell and bicarbonate ions exiting the cell. Under these assumptions, they expressed the BCE turnover rate by eq. (145),

$$J_{BCE} = n''_{BCE} \frac{k^+_{Cl}k^+_{HCO_3}[Cl]_{M(e)}[HCO3]_{N(i)} - k^-_{Cl}k^-_{HCO_3}[Cl]_{N(i)}[HCO3]_{M(e)}}{k^+_{Cl}[Cl]_{M(e)} + k^+_{HCO_3}[HCO3]_{N(i)} + k^-_{HCO_3}[HCO3]_{M(e)} + k^-_{Cl}[Cl]_{N(i)}} \tag{145}$$

where n''_{BCE} is BCE density per membrane area, k^+_i and k^-_i are the dissociation and association rate constants for the ion $'i'$, respectively. The subscript e or M refers to the exterior space, being either the apical or basolateral compartments.

6.2. Sodium Calcium Exchanger (NCX)

The sodium-calcium exchanger (NCX) is the second most important transporter that mediates calcium ion efflux from the cell. It couples the electrochemical potential energy produced during the favorable transport of the sodium ions to the cell to transport the calcium ions out of the cell against their chemical gradient. This exchanger can also work in a *reverse* direction, which causes the influx movement of the calcium ions [181]. Although their transport stoichiometries have not been determined with certainty, significant numbers of experiments suggest that three

sodium ions drive each calcium ion's transport (efflux) out of the cell (i.e. ${3Na^+}_{out} + {Ca^{2+}}_{in} \rightleftharpoons {3Na^+}_{in} + {Ca^{2+}}_{out}$) [182–184]. Therefore, the NaCa exchanger is known to be electrogenic and voltage-dependent, as it results in the net movement of the positive ions into the cell per cycle.

Mullins et al. in 1977 [185] developed a detailed model to determine the flux transported by NCX exchangers for the cardiac tissue. Their full model is relatively complex and involves many unknown rate coefficients. D. Noble and DiFrancesco in 1985 decreased the number of parameters in Mullins et al.'s model [185] based on the fact that sodium concentration changes are relatively small during the few action potentials [62]. Therefore, D. Noble and DiFrancesco [62] assumed that some of the terms in the Mullins model are constant and drove an intermediate version of the Mullins model. Their model is given in eq. (146).

$$I_{NCX} = k_{NCX}\left(\frac{[Na]_i^{n_{NCX}}[Ca]_o exp\left(\frac{(n_{NCX}-2)rV_mF}{2RT}\right) - [Na]_o^{n_{NCX}}[Ca]_i exp\left(-\frac{(n_{NCX}-2)(1-r)V_mF}{2RT}\right)}{1 + d_{NCX}\left([Na]_o^{n_{NCX}}[Ca]_i + [Na]_i^{n_{NCX}}[Ca]_o\right)}\right) \tag{146}$$

where k_{NCX} is the scaling factor that scales the exchange current for a given energy barrier and determines the magnitude of the current. The value of kNCX varies based on the calcium concentration in the extracellular region and the membrane voltage. r characterizes the position of the energy barrier in the electrical field ($0 < r < 1$) that controls the voltage dependence of the [62, 184, 186], and d_{NCX} is the denominator constant.

k_{NCX} in eq. (146) is not constant and it is a function of reaction rates as well as the concentration of the ions in internal and external regions. A Hill-type instantaneous Ca_i-dependent activation term can be included in modeling NCX in cardiac myocytes and pancreatic β-cells [30, 187]. By considering a Hill-type manner for the dependence of intracellular calcium concentration in addition to considering the stoichiometry of the NaCa exchanger to be $nNa : Ca$, the current through

a general $nNa : Ca$ electrogenic exchanger can be obtained by using eq. (147) [30, 188].

$$\boxed{\begin{aligned} I_{NCX} &= g_{NCX}\Big(\frac{1}{(1+\Big(\frac{K^{Ca}_{NCX,m}}{[Ca]_{i(M)}}\Big)^{\eta_{NCX,h}}}\Big) \\ &\left(\frac{[Na]_i^{n_{NCX}}[Ca]_o exp\left(\frac{(n_{NCX}-2)rV_mF}{2RT}\right) - [Na]_o^{n_{NCX}}[Ca]_i exp\left(-\frac{(n_{NCX}-2)(1-r)V_mF}{2RT}\right)}{1+d_{NCX}\left([Na]_o^{n_{NCX}}[Ca]_i + [Na]_i^{n_{NCX}}[Ca]_o\right)}\right) \end{aligned}} \tag{147}$$

In this equation, g_{NCX} is the NCX conductance, $K^{Ca}_{NCX,m}$ is the intracellular calcium concentration ($[Ca]_i$) for half activation of NCX current, $\eta_{NCX,h}$ is the Hill coefficient for half activation of NCX current, n_{NCX} is the NCX stoichiometry, r is the voltage dependence Eyring rate theory partition parameter, and d_{NCX} is the denominator constant for NCX [30, 188].

In 2001, Weber et al. [186, 189] developed a model that accounts for the asymmetric affinities of the exchangers on the two sides of the membrane and the effect of the calcium and sodium concentrations on the current flux carried by the NCX exchanger. Their model is given by eq. (148).

$$\boxed{\begin{aligned} I_{NCX} &= I^{max}_{NCX}\Big(\frac{1}{1+(\frac{K^{Ca}_{m,NCX}}{[Ca]_{i(M)}})^{\eta_{Hill}}}\Big) \\ &\left(\frac{[Na]_{i(M)}^{n_{NCX}}[Ca]_{N(o)} exp(\frac{rV_mF}{RT}) - [Na]_{N(o)}^{n_{NCX}}[Ca]_{i(M)} exp(-\frac{(1-r)V_mF}{RT})}{\lambda(1+k_{sat}exp(-\frac{(1-r)V_mF}{RT}))}\right) \end{aligned}}$$

$$\begin{aligned} \lambda &= [Na]_o^{n_{NCX}}[Ca]_i + [Na]_i^{n_{NCX}}[Ca]_o + K_{m,Cao}[Na]_i^{n_{NCX}} \\ &+K_{m,Nai}^{n_{NCX}}[Ca]_o(1+\frac{[Ca]_i}{K_{m,Cai}}) + K_{m,Cai}[Na]_o^{n_{NCX}}\left(1+\frac{[Na]_i^{n_{NCX}}}{K_{m,Nai}}\right)^{n_{NCX}} \end{aligned} \tag{148}$$

where I^{max}_{NCX} is the maximal NCX current flux in ($\mu A \mu F$), k_{sat} is a constant in (μM) that represents exchanger saturation, and term λ is defined by eq. (148). In eq. (148) $K_{m,Nae}$, $K_{m,Nai}$, $K_{m,Cae}$, $K_{m,Cai}$ are the binding affinities. These binding affinities are defined as: $K_{m,Cai}$ is the internal calcium half-saturation constant for the NCX in (μM), $K_{m,Cao}$ is the external calcium half-saturation constant for the NCX in (mM), $K_{m,Nai}$ is the internal sodium half-saturation constant for the NCX in (mM), and $K_{m,Nao}$ is the external sodium half-saturation constant for the NCX in (mM) [29, 31, 90, 113, 186, 189].

6.3. Sodium Hydrogen Exchanger (NHE)

The sodium-hydrogen exchanger, summarized as NHE, plays an essential role in maintaining the cell's pH, as it provides the major pathway for acid efflux from the cell [190, 191]. The number of available binding sites on the NHE transporter is limited, and there can be competition for the available binding site of the NHE between H^+ and $NH4^+$ [186, 192, 193].

In 1995, Weinstein [194] developed a kinetic model for NHE to compute the transported fluxes through NHE with ammonium transport. This competitive model is depicted in Figure 21 of [20], where A, B, and C refer to sodium, hydrogen, and ammonium, respectively. The transported fluxes of the sodium, hydrogen, and ammonium can be obtained by using eqs. (149), (150) and (151), respectively.

$$J^{NHE}_{Na^+} = E_t \frac{g^M_{ENa} Na^M (g^N_{EH} H^N + g^N_{ENH4} NH^N_4) - g^N_{ENa} Na^N (g^M_{EH} H^M + g^M_{ENH4} NH^M_4)}{R_M R_{NN} + R_N R_{MM}} \tag{149}$$

$$J^{NHE}_{H^+} = E_t \frac{g^M_{EH} H^M (g^N_{ENa} Na^N + g^N_{ENH4} NH^N_4) - g^N_{EH} H^N (g^M_{ENa} Na^M + g^M_{ENH4} NH^M_4)}{R_M R_{NN} + R_N R_{MM}} \tag{150}$$

$$J^{NHE}_{NH_4^+} = E_t \frac{g^M_{ENH4} NH^M_4 (g^N_{ENa} Na^N + g^N_{EH} H^N) - g^N_{ENH4} NH^N_4 (g^M_{ENa} Na^M + g^M_{EH} H^M)}{R_M R_{NN} + R_N R_{MM}} \tag{151}$$

where $[E]_t = [E]_M + [ENa]_M + [EH]_M + [ENH_4]_M + [E]_N + [ENa]_N + [EH]_N + [ENH_4]_N$ represents the total carrier concentration of the NBCn transporter on either side of the membrane. The superscripts 'M' and 'N' refer to the internal and external sides of the membrane; accordingly, g_{ENa}, g_{EH}, g_{ENH4} are the translocations of the exchanger for the carrier bound to Na^+, H^+, and $NH_4{}^+$, respectively, in units of per second (s^{-1}).

R_M, R_N, R_{MM}, and R_{NN} are the resistance parameters and defined as:

$R_M = 1 + Na^M + H^M + NH^M_4 \mid R_N = 1 + Na^N + H^N + NH^N_4$

$R_{MM} = g^M_{ENa} Na^M + g^M_{EH}\ H^M + g^M_{ENH_4} NH^M_4 \mid R_{NN} = g^N_{ENa} Na^N + g^N_{EH}\ H^N + g^N_{ENH_4} NH^N_4$

K_{ion} is the equilibrium constant of the ion in the unit of *mmol* and the normalized concentrations are:

$Na^M = \frac{[Na]_M}{K^M_{Na}},\quad H^M = \frac{[H]_M}{K^M_H},\quad NH^M_4 = \frac{[NH_4]_M}{K^M_{NH_4}} \mid Na^N = \frac{[Na]_N}{K^N_{Na}},\quad H^N = \frac{[H]_N}{K^N_H},\quad NH^N_4 = \frac{[NH_4]_N}{K^N_{NH_4}}$

In the absence of the competitor, the model depicted in Figure 20 in [20] can provide a better

understanding of the transport mechanism by the Na^+/H^+ exchanger. In this model, A represents the Na^+ cations and B denotes the H^+ ions, and the transported fluxes for sodium and hydrogen ions can be obtained by using eqs. (152) and (153), accordingly [192, 195].

$$\boxed{\mathbf{J}_{\mathbf{Na}}^{\mathbf{NHE}} = E_t \frac{g_{ENa}^M g_{EH}^N (Na^M H^N) - g_{ENa}^N g_{EH}^M (Na^N H^M)}{R_M R_{NN} + R_N R_{MM}}} \tag{152}$$

$$\boxed{\mathbf{J}_{\mathbf{H}}^{\mathbf{NHE}} = E_t \frac{g_{EH}^M g_{ENa}^N (H^M Na^N) - g_{EH}^N g_{ENa}^M (H^N Na^M)}{R_M R_{NN} + R_N R_{MM}}} \tag{153}$$

Sohma et al. (1996) [22] developed a simplified model for the one-to-one transport of sodium and hydrogen ions through the NHE antiporter. Their model is re-driven in Figure 22 of [20], where A refers to Na^+ ions and B denotes the H^+ ions. This model assumes that the empty antiporter does not cross the membrane and the turnover rate constants g_{ENaH} for movement from the M to the N side of the membrane and vice-versa are the same (i.e., $g_{ENaH}^M = g_{ENaH}^N = g_{ENaH}$), and the dissociation constants for each solute on both faces are the same (i.e., $K_{Na}^M = K_{Na}^N = K_{Na}$, $K_H^M = K_H^N = K_H$). In addition, the model assumes that the antiporter has a single binding site for the transported ions and the transported ions compete for the same binding sites.

Under these assumptions, the steady-state turnover rate of the NHE can be derived from eq. (154).

$$\boxed{J_{NHE} = P_{NHE} \frac{([Na]_{M(bl)}[H]_{N(c)} - [Na]_{N(c)}[H]_{M(bl)})}{K_{Na}K_H\Big(\Big(1 + \frac{[Na]_{M(bl)}}{K_{Na}} + \frac{[H]_{M(bl)}}{K_H}\Big)\Big(\frac{[Na]_{N(c)}}{K_{Na}} + \frac{[H]_{N(c)}}{K_H}\Big) + \Big(1 + \frac{[Na]_{N(c)}}{K_{Na}} + \frac{[H]_{N(c)}}{K_H}\Big)\Big(\frac{[Na]_{M(bl)}}{K_{Na}} + \frac{[H]_{M(bl)}}{K_H}\Big)\Big)}} \tag{154}$$

where $P_{NHE} = [E_t]\ g_{NHE}$ represents the membrane permeability coefficient for the sodium-hydrogen exchanger (NHE) in unit of $mol/s/cm^2$ (permeability per 1 cm^2), and K_{Na} and K_H are the dissociation constants in mM unit.

There are several other detailed models for the NHE transport mechanism that are out of the scope of this work, and the interested reader is referred to references [196–199].

7. Discussion and Conclusion

Mathematical and computational modeling of the ion channels and membrane transporters are widely acknowledged for examining each transporter's mechanism, the interactions between different transporters, estimating the changes and uncertainties in outcomes, reproducing and analyzing the experimental data, and predicting any new phenomena caused by membrane disorders. Mathematical models are also useful for identifying drug targets and recognizing key control points that would be useful for drug screening trials.

The present work aimed to consolidate the mathematical models that have been developed for the specific types of ion channels and membrane transporters across the cell membrane in one paper. To this end, literature searches were performed to identify studies aiming to drive mathematical models for the ion channels and membrane transporters, and each model was then transformed into a general identical parametric form. The mathematical models describing transport mechanisms through the ion channels and membrane carriers were discussed, and the controlling parameters required for these models were highlighted. Some ion channels are better modeled using linear Ohm models, and some are modeled using the Goldman-Hodgkin-Katz model. The nonlinear Goldman-Hodgkin-Katz model and the linear Ohmic model for ion channels including chloride channels (CaCC, CFTR), potassium channels (IRKC, CaKC, VGPC), sodium channels (NaC, NaV), and calcium channels (SOC, L-type, T-type, VGCC) were presented. Ion channel models were mostly classified based on their current and voltage relationships. Ohm's law is mainly better used to consider a nonzero resting potential difference across the plasma membrane of cells. The detailed gating models for the current through voltage-sensitive ion channels (which respond to membrane electric potential variation) and concentration-dependent ion channels (which open in response to stimuli such as ATP or calcium concentrations) were discussed.

In the same fashion, various available kinetic models for different pumps, symporters, and antiporters were presented. These transporters were categorized into various groups, and available models for their function's quantitative descriptions were provided. Models for ATPase pumps, such as H ATPase (v-type, H/K ATPase), calcium ATPase pump (Ca-ATPase, PMCA, SERCA), and sodium-potassium ATPase pump (Na-K ATPase), are presented. Models for symporters such

as sodium-potassium-chloride symporter (NKCC), chloride potassium symporter (KCC), sodium chloride symporter (NaCl), sodium bicarbonate symporter (NBC), sodium-phosphate symporter (NaPO-4), sodium-glucose transporter (SGLT), and amino acid transporter and antiporters such as chloride bicarbonate exchanger (BCE), sodium-calcium exchanger (NCX), and sodium-hydrogen exchanger (NHE) were presented. Carrier-mediated transport mechanisms such as symporters, antiporters, and pumps were described by using kinetic reaction equations, and the thermal behavior of the transporting molecules was captured in the reaction rate coefficients. These models are experimentally traceable, which allows them to be used as reflective tools to examine the behavior of transporters and make predictions. Moreover, they describe how the transported substrate's apparent affinity is affected by the co-ion concentration and vice versa in different mechanisms.
Both detailed and simplified models were provided to facilitate selecting the appropriate kinetic model for transforming the experimentally obtained kinetic data for each specific type of transporter. The differences among different models arose from the binding and unbinding order of the solutes and the assumptions applied for various reaction steps. Depending on the scientist's expertise, the study's purpose, the knowledge of the model parameters, and the desired level of complexity of the systems to be modeled, one or more of these models may be applied.

In conclusion, mathematical and quantitative studies of membrane transporter mechanisms and ion channels can play a significant role in guiding efforts to optimize new techniques in preventing, diagnosing, and treating diseases caused by membrane disorders and engineering drug delivery. Furthermore, mathematical and computational modeling of membrane transporters has provided an excellent opportunity to improve communication between scientists with different backgrounds in the physiology community and holds tremendous promise for biomedical research. The present work intended to unite the previously done works in mathematical modeling of membrane transporter mechanisms and ion channel fields and to shed light on new research directions for future studies on this topic. We hope that scientists can use this work as a suitable tool for theoretical simulation and analysis of the transporters' cooperative work and engineer the mechanism and interaction of individual membrane transporters more conveniently.

References

References

[1] G. Diallinas, Understanding transporter specificity and the discrete appearance of channel-like gating domains in transporters, Frontiers in pharmacology 5 (2014) 207.

[2] C. D. Klaassen, L. M. Aleksunes, Xenobiotic, bile acid, and cholesterol transporters: function and regulation, Pharmacological reviews 62 (1) (2010) 1–96.

[3] W. W. Wang, L. Gallo, A. Jadhav, R. Hawkins, C. G. Parker, The druggability of solute carriers, Journal of medicinal chemistry (2019).

[4] E. Rebane, Y. N. Orlov, Mathematical model of cooperative work of ion pump, symport and antiport in epithelial cells, Journal of evolutionary biochemistry and physiology 44 (1) (2008) 36–43.

[5] A. S. Kristensen, J. Andersen, T. N. Jørgensen, L. Sørensen, J. Eriksen, C. J. Loland, K. Strømgaard, U. Gether, Slc6 neurotransmitter transporters: structure, function, and regulation, Pharmacological reviews 63 (3) (2011) 585–640.

[6] L. S. King, P. Agre, Pathophysiology of the aquaporin water channels, Annual Review of Physiology 58 (1) (1996) 619–648.

[7] F. M. Ashcroft, Ion channels and disease, Academic press, 1999.

[8] M. A. Hediger, B. Clémençon, R. E. Burrier, E. A. Bruford, The abcs of membrane transporters in health and disease (slc series): introduction, Molecular aspects of medicine 34 (2-3) (2013) 95–107.

[9] A. Aperia, Membrane transport proteins in health and disease, Journal of internal medicine 261 (1) (2007) 2–4.

[10] W. Materi, D. S. Wishart, Computational systems biology in drug discovery and development: methods and applications, Drug discovery today 12 (7-8) (2007) 295–303.

[11] V. Burtscher, K. Schicker, M. Freissmuth, W. Sandtner, Kinetic models of secondary active transporters, International journal of molecular sciences 20 (21) (2019) 5365.

[12] G. A. Fitzgerald, C. Mulligan, J. A. Mindell, A general method for determining secondary active transporter substrate stoichiometry, Elife 6 (2017) e21016.

[13] O. D. Kim, M. Rocha, P. Maia, A review of dynamic modeling approaches and their application in computational strain optimization for metabolic engineering, Frontiers in microbiology 9 (2018) 1690.

[14] G. Penkler, F. Du Toit, W. Adams, M. Rautenbach, D. C. Palm, D. D. Van Niekerk, J. L. Snoep, Construction and validation of a detailed kinetic model of glycolysis in plasmodium falciparum, The FEBS journal 282 (8) (2015) 1481–1511.

[15] P. Bisignano, M. A. Lee, A. George, D. M. Zuckerman, M. Grabe, J. M. Rosenberg, A kinetic mechanism for enhanced selectivity of membrane transport, PLOS Computational Biology 16 (7) (2020) e1007789.

[16] H. Murer, I. Forster, J. Biber, The sodium phosphate cotransporter family slc34, Pflügers Archiv 447 (5) (2004) 763–767.

[17] D. Chen, G. Wei, A review of mathematical modeling, simulation and analysis of membrane channel charge transport, arXiv preprint arXiv:1611.04573 (2016).

[18] J. S. Lolkema, D.-J. Slotboom, The hill analysis and co-ion–driven transporter kinetics, The Journal of general physiology 145 (6) (2015) 565–574.

[19] B. Alberts, A. Johnson, J. Lewis, M. Raff, K. Roberts, P. Walter, Principles of membrane transport, in: Molecular Biology of the Cell. 4th edition, Garland Science, 2002.

[20] S. Zaheri, F. Hassanipour, A comprehensive approach to the mathematical modeling of mass transport in biological systems: Fundamental concepts and models, International Journal of Heat and Mass Transfer 158 (2020) 119777.

[21] P. T. Bonar, J. R. Casey, Plasma membrane cl-/hco3-exchangers: structure, mechanism and physiology, Channels 2 (5) (2008) 337–345.

[22] Y. Sohma, M. Gray, Y. Imai, B. Argent, A mathematical model of the pancreatic ductal epithelium, The Journal of membrane biology 154 (1) (1996) 53–67.

[23] T. E. Andreoli, D. D. Fanestil, J. F. Hoffman, S. G. Schultz, Physiology of membrane disorders, Springer Science & Business Media, 2013.

[24] B. Hille, W. Schwarz, Potassium channels as multi-ion single-file pores., The Journal of General Physiology 72 (4) (1978) 409–442.

[25] G. L. Fain, Molecular and cellular physiology of neurons, Harvard University Press, 1999.

[26] F. Edwards, G. Hirst, G. Silverberg, Inward rectification in rat cerebral arterioles; involvement of potassium ions in autoregulation., The Journal of Physiology 404 (1) (1988) 455–466.

[27] E. E. Benarroch, Potassium channels brief overview and implications in epilepsy, Neurology 72 (7) (2009) 664–669.

[28] J. Quayle, C. Dart, N. Standen, The properties and distribution of inward rectifier potassium currents in pig coronary arterial smooth muscle., The Journal of physiology 494 (3) (1996) 715–726.

[29] A. Edwards, T. L. Pallone, Modification of cytosolic calcium signaling by subplasmalemmal microdomains, American Journal of Physiology-Renal Physiology 292 (6) (2007) F1827–F1845.

[30] H. S. Silva, A. Kapela, N. M. Tsoukias, A mathematical model of plasma membrane electrophysiology and calcium dynamics in vascular endothelial cells, American Journal of Physiology-Cell Physiology 293 (1) (2007) C277–C293.

[31] J. Yang, J. W. Clark Jr, R. M. Bryan, C. Robertson, The myogenic response in isolated rat cerebrovascular arteries: smooth muscle cell model, Medical engineering & physics 25 (8) (2003) 691–709.

[32] S. K. Roberts, M. Tester, Inward and outward k+-selective currents in the plasma membrane of protoplasts from maize root cortex and stele, The Plant Journal 8 (6) (1995) 811–825.

[33] Y. Berwald-Netter, A. Koulakoff, L. Nowak, P. Ascher, Ionic channels in glial cells, Astrocytes. Biochemistry,

Physiology, and Pharmacology of Astrocytes, ed. Fedoroff, S, Vernadakis, A (2012) 51–75.

[34] S. Y. Lee, M. L. Palmer, P. J. Maniak, S. H. Jang, P. D. Ryu, S. M. O'Grady, P2y receptor regulation of sodium transport in human mammary epithelial cells, American Journal of Physiology-Cell Physiology 293 (5) (2007) C1472–C1480.

[35] N. Warren, M. Tawhai, E. Crampin, A mathematical model of calcium-induced fluid secretion in airway epithelium, Journal of theoretical biology 259 (4) (2009) 837–849.

[36] S. Fong, J. A. Chiorini, J. Sneyd, V. Suresh, Computational modeling of epithelial fluid and ion transport in the parotid duct after transfection of human aquaporin-1, American Journal of Physiology-Gastrointestinal and Liver Physiology 312 (2) (2016) G153–G163.

[37] L. Palk, J. Sneyd, T. J. Shuttleworth, D. I. Yule, E. J. Crampin, A dynamic model of saliva secretion, Journal of theoretical biology 266 (4) (2010) 625–640.

[38] T. Hartmann, A. Verkman, Model of ion transport regulation in chloride-secreting airway epithelial cells. integrated description of electrical, chemical, and fluorescence measurements, Biophysical journal 58 (2) (1990) 391–401.

[39] J. Schmid, B. Müller, D. Heppeler, D. Gaynullina, M. Kassmann, H. Gagov, M. Mladenov, M. Gollasch, R. Schubert, The unexpected role of calcium-activated potassium channels: limitation of no-induced arterial relaxation, Journal of the American Heart Association 7 (7) (2018) e007808.

[40] M. J. Davis, M. A. Hill, Signaling mechanisms underlying the vascular myogenic response, Physiological reviews 79 (2) (1999) 387–423.

[41] J. E. Brayden, Potassium channels in vascular smooth muscle, Clinical and experimental pharmacology and physiology 23 (12) (1996) 1069–1076.

[42] Y. Wang, D. Mathers, Ca (2+)-dependent k+ channels of high conductance in smooth muscle cells isolated from rat cerebral arteries., The Journal of physiology 462 (1) (1993) 529–545.

[43] K. Jeevaratnam, K. R. Chadda, C. L.-H. Huang, A. J. Camm, Cardiac potassium channels: physiological insights for targeted therapy, Journal of Cardiovascular Pharmacology and Therapeutics 23 (2) (2018) 119–129.

[44] R. Blunck, Z. Batulan, Mechanism of electromechanical coupling in voltage-gated potassium channels, Frontiers in pharmacology 3 (2012) 166.

[45] A. Hodgkin, A. Huxley, A quantitative description of membrane current and its application to conduction and excitation in nerve, Bulletin of mathematical biology 52 (1-2) (1990) 25–71.

[46] H.-s. Sun, Z.-p. Feng, Neuroprotective role of atp-sensitive potassium channels in cerebral ischemia, Acta Pharmacologica Sinica 34 (1) (2013) 24–32.

[47] A. Tinker, Q. Aziz, A. Thomas, The role of atp-sensitive potassium channels in cellular function and protection in the cardiovascular system, British journal of pharmacology 171 (1) (2014) 12–23.

[48] M. Remedi, C. Nichols, Katp channels in the pancreas: Hyperinsulinism and diabetes, in: Ion Channels in Health and Disease, Elsevier, 2016, pp. 199–221.

[49] Z. Issa, J. M. Miller, D. P. Zipes, Clinical Arrhythmology and Electrophysiology: A Companion to Braunwald's Heart Disease E-Book: Expert Consult: Online and Print, Elsevier Health Sciences, 2012.

[50] M.-L. Zhuo, Y. Huang, D.-P. Liu, C.-C. Liang, Katp channel: relation with cell metabolism and role in the cardiovascular system, The international journal of biochemistry & cell biology 37 (4) (2005) 751–764.

[51] R. M. Shaw, Y. Rudy, Electrophysiologic effects of acute myocardial ischemia: a theoretical study of altered cell excitability and action potential duration, Cardiovascular research 35 (2) (1997) 256–272.

[52] S. C. Yost, Potassium channels basic aspects, functional roles, and medical significance, Anesthesiology: The Journal of the American Society of Anesthesiologists 90 (4) (1999) 1186–1203.

[53] F. Lesage, M. Lazdunski, Molecular and functional properties of two-pore-domain potassium channels, American Journal of Physiology-Renal Physiology 279 (5) (2000) F793–F801.

[54] S. A. Goldstein, D. A. Bayliss, D. Kim, F. Lesage, L. D. Plant, S. Rajan, International union of pharmacology. lv. nomenclature and molecular relationships of two-p potassium channels, Pharmacological reviews 57 (4) (2005) 527–540.

[55] C. Lim, T. Dudev, Potassium versus sodium selectivity in monovalent ion channel selectivity filters, in: The Alkali Metal Ions: Their Role for Life, Springer, 2016, pp. 325–347.

[56] C. M. Canessa, A.-M. Merillat, B. C. Rossier, Membrane topology of the epithelial sodium channel in intact cells, American Journal of Physiology-Cell Physiology 267 (6) (1994) C1682–C1690.

[57] C. Duc, N. Farman, C. M. Canessa, J.-P. Bonvalet, B. C. Rossier, Cell-specific expression of epithelial sodium channel alpha, beta, and gamma subunits in aldosterone-responsive epithelia from the rat: localization by in situ hybridization and immunocytochemistry., The Journal of cell biology 127 (6) (1994) 1907–1921.

[58] Z. Zhang, C. Cao, W. Lee-Kwon, T. L. Pallone, Descending vasa recta pericytes express voltage operated na+ conductance in the rat, The Journal of physiology 567 (2) (2005) 445–457.

[59] C.-h. Luo, Y. Rudy, A model of the ventricular cardiac action potential. depolarization, repolarization, and their interaction., Circulation research 68 (6) (1991) 1501–1526.

[60] L. Ebihara, E. Johnson, Fast sodium current in cardiac muscle. a quantitative description, Biophysical journal 32 (2) (1980) 779–790.

[61] G. W. Beeler, H. Reuter, Reconstruction of the action potential of ventricular myocardial fibres, The Journal of physiology 268 (1) (1977) 177–210.

[62] D. Di Francesco, D. Noble, A model of cardiac electrical activity incorporating ionic pumps and concentration changes, Phil. Trans. R. Soc. Lond. B 307 (1133) (1985) 353–398.

[63] K. Ten Tusscher, D. Noble, P.-J. Noble, A. V. Panfilov, A model for human ventricular tissue, American Journal of Physiology-Heart and Circulatory Physiology 286 (4) (2004) H1573–H1589.

[64] H. Eyring, The activated complex in chemical reactions, The Journal of Chemical Physics 3 (2) (1935) 107–115.

[65] F. H. Johnson, H. Eyring, B. J. Stover, The theory of rate processes in biology and medicine, Wiley-Interscience, 1974.

[66] E. McCleskey, A. Fox, D. Feldman, R. Tsien, Different types of calcium channels, Journal of experimental biology 124 (1) (1986) 177–190.

[67] R. J. Miller, Multiple calcium channels and neuronal function, Science 235 (4784) (1987) 46–52.

[68] A. B. Parekh, J. W. Putney Jr, Store-operated calcium channels, Physiological reviews 85 (2) (2005) 757–810.

[69] A. P. LeBeau, F. Van Goor, S. S. Stojilkovic, A. Sherman, Modeling of membrane excitability in gonadotropin-releasing hormone-secreting hypothalamic neurons regulated by ca2+-mobilizing and adenylyl cyclase-coupled receptors, Journal of Neuroscience 20 (24) (2000) 9290–9297.

[70] C. F. Chen, P. Hess, Mechanism of gating of t-type calcium channels., The Journal of General Physiology 96 (3) (1990) 603–630. arXiv:http://jgp.rupress.org/content/96/3/603.full.pdf, doi:10.1085/jgp.96.3.603.
URL http://jgp.rupress.org/content/96/3/603

[71] J. Huguenard, D. Prince, A novel t-type current underlies prolonged ca (2+)-dependent burst firing in gabaergic neurons of rat thalamic reticular nucleus, Journal of Neuroscience 12 (10) (1992) 3804–3817.

[72] K. Talavera, B. Nilius, Biophysics and structure–function relationship of t-type ca2+ channels, Cell calcium 40 (2) (2006) 97–114.

[73] W. A. Catterall, Voltage-gated calcium channels, Cold Spring Harbor perspectives in biology (2011) a003947.

[74] T. P. Snutch, J. Peloquin, E. Mathews, J. E. McRory, Molecular properties of voltage-gated calcium channels, in: Voltage-gated calcium channels, Springer, 2005, pp. 61–94.

[75] L. Wright, C. Pope, J. Liu, The nervous system as a target for chemical warfare agents, in: Handbook of Toxicology of Chemical Warfare Agents, Elsevier, 2009, pp. 463–480.

[76] E. F. Stanley, Presynaptic calcium channels: why is p selected before n?, Biophysical journal 108 (3) (2015) 451.

[77] J. W. Putney Jr, Calcium signaling, CRC Press, 2005.

[78] M. I. Zhang, R. G. O'Neil, The diversity of calcium channels and their regulation in epithelial cells, Advances in pharmacology 46 (1999) 43–83.

[79] L. G. Navar, W. J. Arendshorst, T. L. Pallone, E. W. Inscho, J. D. Imig, P. D. Bell, The renal microcirculation, Handbook of Physiology: Microcirculation 2 (2008) 550–683.

[80] N. Xu, D. L. Cioffi, M. Alexeyev, T. C. Rich, T. Stevens, Sodium entry through endothelial store-operated calcium entry channels: regulation by orai1, American Journal of Physiology-Cell Physiology 308 (4) (2014) C277–C288.

[81] B. A. Bicknell, G. J. Goodhill, Emergence of ion channel modal gating from independent subunit kinetics,

Proceedings of the National Academy of Sciences 113 (36) (2016) E5288–E5297.

[82] S. Chowdhury, B. Chanda, Free-energy relationships in ion channels activated by voltage and ligand, The Journal of general physiology 141 (1) (2013) 11–28.

[83] G. W. De Young, J. Keizer, A single-pool inositol 1, 4, 5-trisphosphate-receptor-based model for agonist-stimulated oscillations in ca2+ concentration., Proceedings of the National Academy of Sciences 89 (20) (1992) 9895–9899.

[84] D.-O. D. Mak, S. McBride, J. K. Foskett, Inositol 1, 4, 5-tris-phosphate activation of inositol tris-phosphate receptor ca2+ channel by ligand tuning of ca2+ inhibition, Proceedings of the National Academy of Sciences 95 (26) (1998) 15821–15825.

[85] J. Sneyd, M. Falcke, Models of the inositol trisphosphate receptor, Progress in biophysics and molecular biology 89 (3) (2005) 207–245.

[86] P. A. Spiro, H. G. Othmer, The effect of heterogeneously-distributed ryr channels on calcium dynamics in cardiac myocytes, Bulletin of mathematical biology 61 (4) (1999) 651–681.

[87] M. S. Jafri, J. J. Rice, R. L. Winslow, Cardiac ca2+ dynamics: the roles of ryanodine receptor adaptation and sarcoplasmic reticulum load, Biophysical journal 74 (3) (1998) 1149–1168.

[88] T. Feng, S. Kalyaanamoorthy, K. Barakat, L-type calcium channels: Structure and functions, Ion Channels in Health and Sickness (2018) 127.

[89] S. G. Tewari, The sodium pump controls the frequency of action-potential-induced calcium oscillations, Computational & Applied Mathematics 31 (2) (2012) 283–304.

[90] T. R. Shannon, F. Wang, J. Puglisi, C. Weber, D. M. Bers, A mathematical treatment of integrated ca dynamics within the ventricular myocyte, Biophysical journal 87 (5) (2004) 3351–3371.

[91] J. R. Huguenard, D. A. McCormick, Simulation of the currents involved in rhythmic oscillations in thalamic relay neurons, Journal of neurophysiology 68 (4) (1992) 1373–1383.

[92] A. Destexhe, J. R. Huguenard, Modeling voltage-dependent channels, Computational modeling methods for neuroscientists. MIT Press, Cambridge (2010) 107–137.

[93] X.-J. Wang, J. Rinzel, M. A. Rogawski, A model of the t-type calcium current and the low-threshold spike in thalamic neurons, Journal of neurophysiology 66 (3) (1991) 839–850.

[94] D. A. Coulter, J. R. Huguenard, D. A. Prince, Calcium currents in rat thalamocortical relay neurones: kinetic properties of the transient, low-threshold current., The Journal of physiology 414 (1) (1989) 587–604.

[95] J. M. Kowalewski, P. Uhlén, H. Kitano, H. Brismar, Modeling the impact of store-operated ca2+ entry on intracellular ca2+ oscillations, Mathematical biosciences 204 (2) (2006) 232–249.

[96] C. Hartzell, I. Putzier, J. Arreola, Calcium-activated chloride channels, Annu. Rev. Physiol. 67 (2005) 719–758.

[97] J. Arreola, J. E. Melvin, T. Begenisich, Activation of calcium-dependent chloride channels in rat parotid acinar cells., The Journal of general physiology 108 (1) (1996) 35–47.

[98] E. Gin, E. J. Crampin, D. A. Brown, T. J. Shuttleworth, D. I. Yule, J. Sneyd, A mathematical model of fluid secretion from a parotid acinar cell, Journal of theoretical biology 248 (1) (2007) 64–80.

[99] Q.-Z. Fang, N. Zhong, Y. Zhang, Z.-N. Zhou, Tetrandrine inhibits ca2+-activated chloride channel in cultured human umbilical vein endothelial cells., Acta Pharmacologica Sinica 25 (3) (2004) 327–333.

[100] R. Greger, R. Schreiber, M. Mall, A. Wissner, A. Hopf, M. Briel, M. Bleich, R. Warth, K. Kunzelmann, Cystic fibrosis and cftr, Pfluegers Archiv 443 (1) (2001) S3–S7.

[101] S. Blaug, K. Hybiske, J. Cohn, G. L. Firestone, T. E. Machen, S. S. Miller, Enac-and cftr-dependent ion and fluid transport in mammary epithelia, American Journal of Physiology-Cell Physiology 281 (2) (2001) C633–C648.

[102] S. Moon, M. Singh, M. E. Krouse, J. J. Wine, Calcium-stimulated cl- secretion in calu-3 human airway cells requires cftr, American Journal of Physiology-Lung Cellular and Molecular Physiology 273 (6) (1997) L1208–L1219.

[103] D. C. Whitcomb, G. B. Ermentrout, A mathematical model of the pancreatic duct cell generating high bicarbonate concentrations in pancreatic juice, Pancreas 29 (2) (2004) e30–e40.

[104] R. J. Roselli, K. R. Diller, Biotransport: principles and applications, Springer Science & Business Media, 2011.

[105] J. L. Tymoczko, J. M. Berg, L. Stryer, Biochemistry: a short course, Macmillan, 2011.

[106] K. Thorsen, T. Drengstig, P. Ruoff, Transepithelial glucose transport and na+/k+ homeostasis in enterocytes: an integrative model, American Journal of Physiology-Cell Physiology 307 (4) (2014) C320–C337.

[107] P. Oliveira, A. R. Da Costa, H. Ferreira, A mathematical model of the proton balance in the outer mantle epithelium of anodonta cygnea l., Journal of Membrane Biology 223 (2) (2008) 59–72.

[108] P. Hoffman, D. Tosteson, Active sodium and potassium transport in high potassium and low potassium sheep red cells, The Journal of general physiology 58 (4) (1971) 438–466.

[109] J. Strieter, J. L. Stephenson, G. Giebisch, A. M. Weinstein, A mathematical model of the rabbit cortical collecting tubule, American Journal of Physiology-Renal Physiology 263 (6) (1992) F1063–F1075.

[110] R. Garay, P. Garrahan, The interaction of sodium and potassium with the sodium pump in red cells, The Journal of Physiology 231 (2) (1973) 297–325.

[111] A. M. Weinstein, A mathematical model of the inner medullary collecting duct of the rat: acid/base transport, American Journal of Physiology-Renal Physiology 274 (5) (1998) F856–F867.

[112] A. M. Weinstein, A mathematical model of rat ascending henle limb. i. cotransporter function, American Journal of Physiology-Renal Physiology 298 (3) (2010) F512–F524.

[113] C.-h. Luo, Y. Rudy, A dynamic model of the cardiac ventricular action potential. i. simulations of ionic currents and concentration changes., Circulation research 74 (6) (1994) 1071–1096.

[114] N. Smith, E. Crampin, Development of models of active ion transport for whole-cell modelling: cardiac sodium–potassium pump as a case study, Progress in biophysics and molecular biology 85 (2-3) (2004) 387–

405.

[115] O. Andersen, J. Silveira, P. Steinmetz, Intrinsic characteristics of the proton pump in the luminal membrane of a tight urinary epithelium. the relation between transport rate and delta mu h., The Journal of general physiology 86 (2) (1985) 215–234.

[116] M. Nadal-Quirós, L. C. Moore, M. Marcano, Parameter estimation for mathematical models of a nongastric h+ (na+)-k+ (nh4+)-atpase, American Journal of Physiology-Renal Physiology 309 (5) (2015) F434–F446.

[117] I. Mangialavori, A. M. V. Giraldo, M. F. Pignataro, M. F. Gomes, A. J. Caride, J. P. F. Rossi, Pmca differential exposure of hydrophobic domains after calmodulin and phosphatidic acid activation, Journal of Biological Chemistry (2011) jbc–M110.

[118] J. N. VanHouten, M. C. Neville, J. J. Wysolmerski, The calcium-sensing receptor regulates plasma membrane calcium adenosine triphosphatase isoform 2 activity in mammary epithelial cells: a mechanism for calcium-regulated calcium transport into milk, Endocrinology 148 (12) (2007) 5943–5954.

[119] T. A. Reinhardt, J. D. Lippolis, Bovine milk fat globule membrane proteome, Journal of Dairy Research 73 (4) (2006) 406–416.

[120] M. S. Ferreira-Gomes, R. M. González-Lebrero, C. María, E. E. Strehler, R. C. Rossi, J. P. F. Rossi, Calcium occlusion in plasma membrane ca2+-atpase, Journal of Biological Chemistry 286 (37) (2011) 32018–32025.

[121] A. Edwards, O. Bonny, A model of calcium transport and regulation in the proximal tubule, American Journal of Physiology-Renal Physiology (2018).

[122] E. Graf, J. T. Penniston, Equimolar interaction between calmodulin and the ca2+ atpase from human erythrocyte membranes, Archives of biochemistry and biophysics 210 (1) (1981) 257–262.

[123] Y. Kojiro, O. H. Petersen, A. V. Tepikin, Dual sensitivity of sarcoplasmic/endoplasmic ca2+-atpase to cytosolic and endoplasmic reticulum ca2+ as a mechanism of modulating cytosolic ca2+ oscillations, Biochemical Journal 383 (2) (2004) 353–360.

[124] E. R. Higgins, M. B. Cannell, J. Sneyd, A buffering serca pump in models of calcium dynamics, Biophysical journal 91 (1) (2006) 151–163.

[125] J. T. Koivumäki, J. Takalo, T. Korhonen, P. Tavi, M. Weckström, Modelling sarcoplasmic reticulum calcium atpase and its regulation in cardiac myocytes, Philosophical Transactions of the Royal Society of London A: Mathematical, Physical and Engineering Sciences 367 (1896) (2009) 2181–2202.

[126] H. L. Baker, R. J. Errington, S. C. Davies, A. K. Campbell, A mathematical model predicts that calreticulin interacts with the endoplasmic reticulum ca2+-atpase, Biophysical journal 82 (2) (2002) 582–590.

[127] C. J. Favre, J. Schrenzel, J. Jacquet, D. P. Lew, K.-H. Krause, Highly supralinear feedback inhibition of ca2+ uptake by the ca2+ load of intracellular stores, Journal of Biological Chemistry 271 (25) (1996) 14925–14930.

[128] J. Sneyd, K. Tsaneva-Atanasova, J. Bruce, S. Straub, D. Giovannucci, D. Yule, A model of calcium waves in pancreatic and parotid acinar cells, Biophysical journal 85 (3) (2003) 1392–1405.

[129] T. R. Shannon, K. S. Ginsburg, D. M. Bers, Reverse mode of the sarcoplasmic reticulum calcium pump and load-dependent cytosolic calcium decline in voltage-clamped cardiac ventricular myocytes, Biophysical journal 78 (1) (2000) 322–333.

[130] F. P. Diecke, Q. Wen, P. Iserovich, J. Li, K. Kuang, J. Fischbarg, Regulation of na–k–2cl cotransport in cultured bovine corneal endothelial cells, Experimental eye research 80 (6) (2005) 777–785.

[131] J. M. Russell, Sodium-potassium-chloride cotransport, Physiological reviews 80 (1) (2000) 211–276.

[132] S. N. Orlov, S. V. Koltsova, L. V. Kapilevich, S. V. Gusakova, N. O. Dulin, Nkcc1 and nkcc2: The pathogenetic role of cation-chloride cotransporters in hypertension, Genes & diseases 2 (2) (2015) 186–196.

[133] L. D'Andrea, C. Lytle, J. B. Matthews, P. Hofman, B. Forbush, J. L. Madara, Na: K: 2cl cotransporter (nkcc) of intestinal epithelial cells surface expression in response to camp, Journal of Biological Chemistry 271 (46) (1996) 28969–28976.

[134] L. M. Iwamoto, N. Fujiwara, K. T. Nakamura, R. K. Wada, Na-k-2cl cotransporter inhibition impairs human lung cellular proliferation, American Journal of Physiology-Lung Cellular and Molecular Physiology 287 (3) (2004) L510–L514.

[135] C. Lytle, J.-C. Xu, D. Biemesderfer, B. Forbush 3rd, Distribution and diversity of na-k-cl cotransport proteins: a study with monoclonal antibodies, American Journal of Physiology-Cell Physiology 269 (6) (1995) C1496–C1505.

[136] C. Lytle, T. J. McManus, M. Haas, A model of na-k-2cl cotransport based on ordered ion binding and glide symmetry, American Journal of Physiology-Cell Physiology 274 (2) (1998) C299–C309.

[137] E. Delpire, K. B. Gagnon, Kinetics of hyperosmotically stimulated na-k-2cl cotransporter in xenopus laevis oocytes, American Journal of Physiology-Cell Physiology 301 (5) (2011) C1074–C1085.

[138] N. Markadieu, E. Delpire, Physiology and pathophysiology of slc12a1/2 transporters, Pflügers Archiv-European Journal of Physiology 466 (1) (2014) 91–105.

[139] B. Benjamin, E. Johnson, A quantitative description of the NaK2Cl cotransporter and its conformity to experimental data, American Journal of Physiology-Renal Physiology 273 (3) (1997) F473–F482.

[140] M. Marcano, H.-M. Yang, A. Nieves-González, C. Clausen, L. C. Moore, Parameter estimation for mathematical models of nkcc2 cotransporter isoforms, American Journal of Physiology-Renal Physiology 296 (2) (2009) F369–F381.

[141] A. M. Weinstein, A mathematical model of rat ascending henle limb. i. cotransporter function, American Journal of Physiology-Renal Physiology 298 (3) (2009) F512–F524.

[142] A. Verkman, R. J. Alpern, Kinetic transport model for cellular regulation of ph and solute concentration in the renal proximal tubule, Biophysical journal 51 (4) (1987) 533–546.

[143] L. Palk, J. Sneyd, K. Patterson, T. J. Shuttleworth, D. I. Yule, O. Maclaren, E. J. Crampin, Modelling the effects of calcium waves and oscillations on saliva secretion, Journal of theoretical biology 305 (2012) 45–53.

[144] F. J. Alvarez-Leefmans, E. Delpire, Thermodynamics and kinetics of chloride transport in neurons: an outline, Physiology and pathology of chloride transporters and channels in the nervous system (Alvarez-Leefmans FJ, Delpire E, eds) (2009) 81–108.

[145] E. L. Boulpaep, W. F. Boron, M. J. Caplan, L. Cantley, P. Igarashi, P. S. Aronson, E. Moczydlowski, Medical physiology a cellular and molecular approach, Signal Transduct 48 (2009) 27.

[146] U. Rudolph, Diversity and functions of GABA receptors: A tribute to Hanns Möhler, Part B, Academic Press, 2015.

[147] D. M. Kaji, Effect of membrane potential on k-cl transport in human erythrocytes, American Journal of Physiology-Cell Physiology 264 (2) (1993) C376–C382.

[148] C. Brugnara, T. Van Ha, D. C. Tosteson, Role of chloride in potassium transport through a k-cl cotransport system in human red blood cells, American Journal of Physiology-Cell Physiology 256 (5) (1989) C994–C1003.

[149] R. A. DeFazio, S. Keros, M. W. Quick, J. J. Hablitz, Potassium-coupled chloride cotransport controls intracellular chloride in rat neocortical pyramidal neurons, Journal of Neuroscience 20 (21) (2000) 8069–8076.

[150] D. W. Good, Ammonium transport by the thick ascending limb of henle's loop, Annual Review of Physiology 56 (1) (1994) 623–647.

[151] I. D. Weiner, L. L. Hamm, Molecular mechanisms of renal ammonia transport, Annu. Rev. Physiol. 69 (2007) 317–340.

[152] L. G. Feld, H. E. Corey, Renal transport of sodium during early development, in: Fetal and neonatal physiology, Elsevier, 2004, pp. 1267–1278.

[153] A. C. Mistry, B. M. Wynne, L. Yu, V. Tomilin, Q. Yue, Y. Zhou, O. Al-Khalili, R. Mallick, H. Cai, A. A. Alli, et al., The sodium chloride cotransporter (ncc) and epithelial sodium channel (enac) associate, Biochemical Journal 473 (19) (2016) 3237–3252.

[154] A. M. Weinstein, A mathematical model of rat distal convoluted tubule. i. cotransporter function in early dct, American Journal of Physiology-Renal Physiology 289 (4) (2005) F699–F720.

[155] I. Choi, C. Aalkjaer, E. L. Boulpaep, W. F. Boron, An electroneutral sodium/bicarbonate cotransporter nbcn1 and associated sodium channel, Nature 405 (6786) (2000) 571–575.

[156] W. F. Boron, Sodium-coupled bicarbonate transporters, Jop 2 (4 Suppl) (2001) 176–181.

[157] H. J. Park, I. Rajbhandari, H. S. Yang, S. Lee, D. Cucoranu, D. S. Cooper, J. D. Klein, J. M. Sands, I. Choi, Neuronal expression of sodium/bicarbonate cotransporter nbcn1 (slc4a7) and its response to chronic metabolic acidosis, American Journal of Physiology-Cell Physiology 298 (5) (2010) C1018–C1028.

[158] C. J. Schwiening, W. F. Boron, Regulation of intracellular ph in pyramidal neurones from the rat hippocampus by na (+)-dependent cl (-)-hco3-exchange., The Journal of Physiology 475 (1) (1994) 59–67.

[159] D. Lagadic-Gossmann, K. Buckler, R. Vaughan-Jones, Role of bicarbonate in ph recovery from intracellular

acidosis in the guinea-pig ventricular myocyte., The Journal of physiology 458 (1) (1992) 361–384.

[160] C. Dart, R. Vaughan-Jones, Na (+)-hco3-symport in the sheep cardiac purkinje fibre., The Journal of Physiology 451 (1) (1992) 365–385.

[161] V. C. De Giusti, A. Orlowski, M. C. Ciancio, M. S. Espejo, L. A. Gonano, C. I. Caldiz, M. G. V. Petroff, M. C. Villa-Abrille, E. A. Aiello, Aldosterone stimulates the cardiac sodium/bicarbonate cotransporter via activation of the g protein-coupled receptor gpr30, Journal of Molecular and Cellular Cardiology 89 (2015) 260–267.

[162] C. C. Aickin, Regulation of intracellular ph in the smooth muscle of guinea-pig ureter: Na+ dependence., The Journal of physiology 479 (2) (1994) 301–316.

[163] C. Aalkjær, A. Hughes, Chloride and bicarbonate transport in rat resistance arteries., The Journal of Physiology 436 (1) (1991) 57–73.

[164] E. Gross, N. Abuladze, A. Pushkin, I. Kurtz, C. Cotton, The stoichiometry of the electrogenic sodium bicarbonate cotransporter pnbc1 in mouse pancreatic duct cells is 2 hco3-: 1 na+, The Journal of Physiology 531 (2) (2001) 375–382.

[165] O. W. Moe, R. T. Miller, S. Horie, A. Cano, P. A. Preisig, R. J. Alpern, Differential regulation of na/h antiporter by acid in renal epithelial cells and fibroblasts., The Journal of clinical investigation 88 (5) (1991) 1703–1708.

[166] J. Prætorius, H. Hager, S. Nielsen, C. Aalkjaer, U. G. Friis, M. A. Ainsworth, T. Johansen, Molecular and functional evidence for electrogenic and electroneutral na+-hco 3- cotransporters in murine duodenum, American Journal of Physiology-Gastrointestinal and Liver Physiology (2001).

[167] Y. Sohma, M. Gray, Y. Imai, B. Argent, Hco 3- transport in a mathematical model of the pancreatic ductal epithelium, The Journal of membrane biology 176 (1) (2000) 77–100.

[168] E. Gross, U. Hopfer, Voltage and cosubstrate dependence of the na-hco3 cotransporter kinetics in renal proximal tubule cells, Biophysical journal 75 (2) (1998) 810–824.

[169] Z. Olah, C. Lehel, W. B. Anderson, M. V. Eiden, C. A. Wilson, The cellular receptor for gibbon ape leukemia virus is a novel high affinity sodium-dependent phosphate transporter., Journal of Biological Chemistry 269 (41) (1994) 25426–25431.

[170] C. Ghezzi, H. Murer, I. C. Forster, Substrate interactions of the electroneutral na+-coupled inorganic phosphate cotransporter (napi-iic), The Journal of physiology 587 (17) (2009) 4293–4307.

[171] C. Fenollar-Ferrer, L. R. Forrest, Structural models of the napi-ii sodium-phosphate cotransporters, Pflügers Archiv-European Journal of Physiology 471 (1) (2019) 43–52.

[172] S. Elmariah, R. B. Gunn, Kinetic evidence that the na-po4 cotransporter is the molecular mechanism for na/li exchange in human red blood cells, American Journal of Physiology-Cell Physiology 285 (2) (2003) C446–C456.

[173] S. B. Poulsen, R. A. Fenton, T. Rieg, Sodium-glucose cotransport, Current opinion in nephrology and hypertension 24 (5) (2015) 463.

[174] S. Eskandari, E. Wright, D. Loo, Kinetics of the reverse mode of the na+/glucose cotransporter, The Journal of membrane biology 204 (1) (2005) 23–32.

[175] D. Loo, A. Hazama, S. Supplisson, E. TuRK, E. M. Wright, Relaxation kinetics of the na+/glucose cotransporter, Proceedings of the National Academy of Sciences 90 (12) (1993) 5767–5771.

[176] W. Stein, The movement of molecules across cell membranes, Vol. 6, Elsevier, 2012.

[177] L. Parent, S. Supplisson, D. D. Loo, E. M. Wright, Electrogenic properties of the cloned na+/glucose cotransporter: Ii. a transport model under nonrapid equilibrium conditions, The Journal of membrane biology 125 (1) (1992) 63–79.

[178] J. Linzell, M. Peaker, The distribution and movements of carbon dioxide, carbonic acid and bicarbonate between blood and milk in the goat., The Journal of physiology 244 (3) (1975) 771–782.

[179] D. Shennan, M. Peaker, Transport of milk constituents by the mammary gland, Physiological reviews 80 (3) (2000) 925–951.

[180] A. M. Weinstein, A mathematical model of the outer medullary collecting duct of the rat, American Journal of Physiology-Renal Physiology 279 (1) (2000) F24–F45.

[181] N. Janvier, M. Boyett, The role of na-ca exchange current in the cardiac action potential, Cardiovascular research 32 (1) (1996) 69–84.

[182] D. Noble, Sodium-calcium exchange and its role in generating electric current, Cardiac muscle: the regulation of excitation and contraction (1986) 171–200.

[183] D. A. Beard, H. Qian, Chemical biophysics: quantitative analysis of cellular systems, Cambridge University Press, 2008.

[184] J. Kimura, S. Miyamae, A. Noma, Identification of sodium-calcium exchange current in single ventricular cells of guinea-pig., The Journal of Physiology 384 (1) (1987) 199–222.

[185] L. Mullins, A mechanism for na/ca transport., The Journal of general physiology 70 (6) (1977) 681–695.

[186] A. T. Layton, A. Edwards, Mathematical Modeling in Renal Physiology, Springer, 2014.

[187] D. Gall, J. Gromada, I. Susa, P. Rorsman, A. Herchuelz, K. Bokvist, Significance of na/ca exchange for ca2+ buffering and electrical activity in mouse pancreatic β-cells, Biophysical journal 76 (4) (1999) 2018–2028.

[188] D. Lindblad, C. Murphey, J. Clark, W. Giles, A model of the action potential and underlying membrane currents in a rabbit atrial cell, American Journal of Physiology-Heart and Circulatory Physiology 271 (4) (1996) H1666–H1696.

[189] C. R. Weber, K. S. Ginsburg, K. D. Philipson, T. R. Shannon, D. M. Bers, Allosteric regulation of na/ca exchange current by cytosolic ca in intact cardiac myocytes, The Journal of general physiology 117 (2) (2001) 119–132.

[190] J. Orlowski, S. Grinstein, Na+/h+ exchangers, Comprehensive Physiology (2011).

[191] E. J. Crampin, N. P. Smith, A dynamic model of excitation-contraction coupling during acidosis in cardiac

ventricular myocytes, Biophysical journal 90 (9) (2006) 3074–3090.

[192] H. Chang, T. Fujita, A numerical model of acid-base transport in rat distal tubule, American Journal of Physiology-Renal Physiology 281 (2) (2001) F222–F243.

[193] P. S. Aronson, Kinetic properties of the plasma membrane na+-h+ exchanger, Annual review of physiology 47 (1) (1985) 545–560.

[194] A. M. Weinstein, A kinetically defined na+/h+ antiporter within a mathematical model of the rat proximal tubule., The Journal of General Physiology 105 (5) (1995) 617–641.

[195] O. Călinescu, C. Paulino, W. Kühlbrandt, K. Fendler, Keeping it simple- transport mechanism and ph regulation in na+/h+ exchangers, Journal of Biological Chemistry (2014) jbc–M113.

[196] K. Otsu, J. Kinsella, B. Sacktor, J. P. Froehlich, Transient state kinetic evidence for an oligomer in the mechanism of na+-h+ exchange, Proceedings of the National Academy of Sciences 86 (13) (1989) 4818–4822.

[197] K. Otsu, J. L. Kinsella, P. Heller, J. P. Froehlich, Sodium dependence of the na (+)-h+ exchanger in the pre-steady state. implications for the exchange mechanism., Journal of Biological Chemistry 268 (5) (1993) 3184–3193.

[198] J. Lacroix, M. Poet, C. Maehrel, L. Counillon, A mechanism for the activation of the na/h exchanger nhe-1 by cytoplasmic acidification and mitogens, EMBO reports 5 (1) (2004) 91–96.

[199] D. Fuster, O. W. Moe, D. W. Hilgemann, Steady-state function of the ubiquitous mammalian na/h exchanger (nhe1) in relation to dimer coupling models with 2na/2h stoichiometry, The Journal of general physiology 132 (4) (2008) 465–480.